JCTC Journal of Chemical Theory and Computation

Article

pubs.acs.org/JCTC

Molecular Dynamics Simulations of Phosphatidylcholine Membranes: A Comparative Force Field Study

Thomas J. Piggot,[†] Ángel Piñeiro,*[,‡] and Syma Khalid*[,†]

[†]School of Chemistry, University of Southampton, Highfield, Southampton, SO17 1BJ, United Kingdom

[‡]Department of Applied Physics, University of Santiago de Compostela, Campus Vida, 15782, Santiago de Compostela, Spain

Supporting Information

ABSTRACT: Molecular dynamics simulations provide a route to studying the dynamics of lipid bilayers at atomistic or near atomistic resolution. Over the past 10 years or so, molecular dynamics simulations have become an established part of the biophysicist's tool kit for the study of model biological membranes. As simulation time scales move from tens to hundreds of nanoseconds and beyond, it is timely to re-evaluate the accuracy of simulation models. We describe a comparative analysis of five freely available force fields that are commonly used to model lipid bilayers. We focus our analysis on 1,2-dipalmitoyl-*sn*-glycero-3-phosphocholine (DPPC) and 1-palmitoyl-2-oleoyl-*sn*-glycero-3-phosphocholine (POPC) bilayers. We show that some bilayer properties have a pronounced force field dependence, while others are less sensitive. In general, we find strengths and weaknesses, with respect to experimental data, in all of the force fields we have studied. We do, however, find some combinations of simulation and force field parameters that should be avoided when simulating DPPC and POPC membranes. We anticipate that the results presented for some of the membrane properties will guide future improvements for several force fields studied in this work.

INTRODUCTION

Over the past 10 years or so, molecular dynamics (MD) simulations have become an established tool for the study of biological membranes and membrane proteins. The atomistic (or more coarse-grain) resolution and ability to probe the dynamics of both the membrane protein and the surrounding environment make MD simulations an ideal complement to structural studies and experimental biophysics. Indeed structural data from X-ray or NMR studies is now routinely used to initiate MD simulations, thus adding dynamics to the static structures enabling prediction of mechanistic details. In addition to probing the protein conformational dynamics, MD simulations provide insights into the interplay between membrane proteins and their local environment, which extends to environments that can be difficult to study with experimental methods.[1] In particular, MD simulations have increased our understanding of membrane proteins in the context of their conformational dynamics, e.g., bacterial outer membrane proteins such as OmpA[2,3] and OprF,[1,4] oligomerization, e.g., of helical proteins and peptides such as glycophorin A and Fukutin-I,[5−7] substrate binding, e.g., to the β_2-adrenergic receptor,[8] and interactions with the local environment, e.g., antimicrobial peptides.[9,10]

Accelerated simulations methods such as metadynamics,[11] accelerated MD,[12,13] and dynamic importance sampling[14,15] have extended the time scales available to atomistic simulations, thereby further increasing their scope and utility. For example, Shimamura et al.[16] recently reported a study in which structural biology, equilibrium molecular dynamics, and dynamic importance sampling was used to propose a mechanism for the transport cycle of the sodium-hydantoin transporter protein, Mhp1 from *M. liquefaciens*.

Recent advances in simulation code efficiency, and the availability of ever-increasing amounts of computational resources, are now enabling atomistic simulations of membranes and membrane proteins that are on the microsecond time scale (e.g., refs 17−19). Thus, as longer trajectories are generated, and we move well beyond the time scales on which the parameters used for proteins and lipids were developed and validated, it is timely to consider the accuracy of the parameters that are used to generate simulation trajectories. Here, we focus our attention on the accuracy of MD simulations of lipid bilayers.

A number of force field parameter sets exist for phospholipids and are shared within the membrane simulation community either by distribution through software packages such as GROMACS[20] or *via* downloads from Web sites. Recently, the Lipidbook web repository developed by Beckstein and co-workers has begun to collate these parameter sets in one online resource.[21] While many parameter sets exist, there is little comparative information available regarding their ability to reproduce experimental lipid bilayer properties. Where comparisons have been made (e.g., refs 22−27), these have tended to focus on either the use of different simulation parameters for a single force field or the comparison between a small number of different force fields.

In the following work, we present a comprehensive comparison of five different force fields for simulating two commonly studied phospholipid bilayers, namely, 1,2-dipalmitoyl-*sn*-glycero-3-phosphocholine (DPPC) and 1-palmitoyl-2-oleoyl-*sn*-glycero-3-phosphocholine (POPC; Figure 1). Our results reveal that many of the equilibrium physical properties

Received: April 18, 2012

   dx.doi.org/10.1021/ct3003157 | *J. Chem. Theory Comput.* XXXX, XXX, XXX−XXX

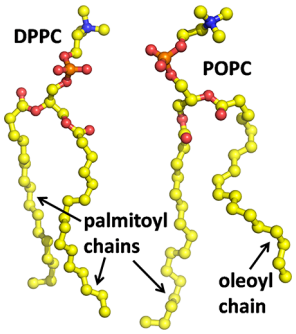

Figure 1. United-atom representations of 1,2-dipalmitoyl-*sn*-glycero-3-phosphocholine (DPPC) and 1-palmitoyl-2-oleoyl-*sn*-glycero-3-phosphocholine (POPC).

of POPC and DPPC bilayers from MD simulations are substantially force field dependent. The various force fields have their own particular strengths and weaknesses.

METHODS

Five freely available force fields, used for the simulation of DPPC and POPC membranes, were compared: GROMOS 43A1-S3,[28] GROMOS 53A6$_L$,[29] Berger,[30] GROMOS 53A6 Kukol,[31] and CHARMM36.[32] Additionally, several modifications were also made to some of the available force field parameters. A discussion of any modifications made to the force fields as well as details of the simulation parameters (e.g., cutoffs) and analysis methods are provided below.

Simulation and Force Field Parameters. All the simulations were performed using the GROMACS simulation package[20,33,34] (version 4.5.1 for CHARMM36 and version 4.0.7 for all other force fields). Prior to simulation, all systems were minimized using the steepest descent method for 1000 steps. The pressure was maintained at 1 bar using the Parrinello−Rahman pressure coupling algorithm[35,36] with a time constant of 5.0 ps. Pressure coupling was applied semi-isotropically, with the z dimension (i.e., perpendicular to the plane of the bilayer) allowed to fluctuate independently of x and y dimensions. For the DPPC bilayer simulations, the temperature was maintained at 323 K and for POPC at 298 K, above the phase transition points in both cases, using the Nosé−Hoover algorithm[37,38] with a time constant of 0.5 ps. Exceptions to this were some of the CHARMM36 POPC bilayer simulations in which the temperature was maintained at 303 K (to match the original CHARMM36 simulations[32]). Simulations in which the long-range electrostatic interactions were treated with the particle mesh Ewald (PME) method[39] used a grid spacing of 0.12 nm with a cubic interpolation. During all simulations, irrespective of the time step, the neighbor list was updated every five steps. All simulations were performed for 200 ns, apart from some of the CHARMM36 simulations that were 100 ns in length (see Table S4 for more details). Repeat simulations, with differently assigned random starting velocities, were performed for all united-atom simulations. Repeat simulations for the CHARMM36 force field used slightly different methods to truncate the van der Waals interactions (see below for further details).

The remaining simulation parameters, which were taken to replicate as closely as possible those used in the original publications of each force field, are discussed in the following sections. Summaries of all the simulations are provided in Table 1 and Supporting Information Table S4.

Table 1. Summary of the Simulations of the Five Force Fields[a]

Force Field	Lipid	Topology Notes	Simulation Notes	Simulation ID*
GROMOS 43A1-S3	DPPC	Standard topology	Coulombic cut-off: 1.0 nm with PME; van der Waals cut-off: 1.0/1.6 nm	S_D1a S_D1b
	POPC			S_P1a S_P1b
GROMOS 53A6$_L$	DPPC	Standard topology	0.8/1.4 nm cut-off with RF	L_D1a L_D1b
	POPC	Downloaded topology (three CH_2-CH_2-N-CH_3 dihedrals)		L_P1a L_P1b
		Corrected topology (one CH_2-CH_2-N-CH_3 dihedral)		L_P2a L_P2b
Berger	DPPC	Downloaded topology	Coulombic cut-off: 1.0 nm with PME; van der Waals cut-off: 1.0 nm plus dispersion correction	B_D1a B_D1b
		Corrected glycerol region dihedrals		B_D2a B_D2b
		Corrected dihedrals and corrected LOS atom type parameters		B_D3a B_D3b
			Coulombic cut-off: 1.0 nm with PME; van der Waals cut-off: 1.0 nm	B_D4a B_D4b
			Coulombic cut-off: 0.9 nm with PME; van der Waals cut-off: 0.9/1.4 nm	B_D5a B_D5b
	POPC	Downloaded topology	Coulombic cut-off: 1.0 nm with PME; van der Waals cut-off: 1.0 nm plus dispersion correction	B_P1a B_P1b
		Corrected dihedrals		B_P2a B_P2b
		Corrected dihedrals and corrected LOS atom type parameters		B_P3a B_P3b
			Coulombic cut-off: 1.0 nm with PME; van der Waals cut-off: 1.0 nm	B_P4a B_P4b
			Coulombic cut-off: 0.9 nm with PME; van der Waals cut-off: 0.9/1.4 nm	B_P5a B_P5b
GROMOS 53A6 Kukol & GROMOS-CKP	DPPC	Standard Kukol topology	0.8/1.4 nm cut-off with RF	K_D2a K_D2b
			Coulombic cut-off: 0.9 nm with PME; van der Waals cut-off: 0.9/1.4 nm plus dispersion correction	K_D1a K_D1b
	POPC			K_P1a K_P1b
		Corrected glycerol region dihedrals		K_P2a K_P2b
		Corrected dihedrals and standard GROMOS double bond parameters (i.e., CKP parameters)		K_P3a K_P3b
			0.8/1.4 nm cut-off with RF	K_P4a K_P4b
CHARMM36	DPPC	Standard topology	Standard TIP3P, 1 fs timestep, neighbor list 1.2 nm, 72 lipids	C_D1a C_D1b
			Standard TIP3P, 1 fs timestep, neighbor list 1.4 nm, 72 lipids	C_D2a C_D2b
			CHARMM TIP3P, 1 fs timestep, neighbor list 1.2 nm, 72 lipids	C_D3a C_D3b
			CHARMM TIP3P, 2 fs timestep neighbor list 1.2 nm, 72 lipids	C_D4a C_D4b
			CHARMM TIP3P, 1 fs timestep, neighbor list 1.4 nm, 72 lipids	C_D5a C_D5b
			CHARMM TIP3P, 1 fs timestep, neighbor list 1.2 nm, 288 lipids	C_D6a C_D6b
	POPC		Standard TIP3P, 1 fs timestep, neighbor list 1.2 nm, 72 lipids	C_P1a C_P1b
			Standard TIP3P, 1 fs timestep, neighbor list 1.4 nm, 72 lipids	C_P2a C_P2b
			CHARMM TIP3P, 1 fs timestep, neighbor list 1.2 nm, 72 lipids	C_P3a C_P3b
			CHARMM TIP3P, 2 fs timestep, neighbor list 1.2 nm, 72 lipids	C_P4a C_P4b
			CHARMM TIP3P, 1 fs timestep, neighbor list 1.4 nm, 72 lipids	C_P5a C_P5b
			CHARMM TIP3P, 1 fs timestep, neighbor list 1.2 nm, 288 lipids	C_P6a C_P6b

[a]A more detailed version of this table is included in the Supporting Information (Table S4). All details of the simulations are also provided in the Methods section, including details of the simulations performed using optimal parameters. [b]For the CHARMM36 force field simulation repeats, simulations labeled 'a' were performed with a value of 0.8 nm used to start switching off the van der Waals interactions; simulations labeled 'b' used a value of 1.1 nm. See the Methods section for further details of the cutoffs employed in the CHARMM36 simulations. For the other force fields, repeat simulations ('a' and 'b') used different starting velocities.

GROMOS 43A1-S3 Force Field. The GROMOS 43A1-S3 lipid force field[28,40] is an extension and modification of the GROMOS 43A1 force field,[41−43] designed to improve the properties of lipid membranes. The charges for phosphatidylcholine (PC) lipids are those as described by Chiu et al.,[44] with the van der Waals and dihedral parameters modified from the standard GROMOS 43A1 force field to improve both

dx.doi.org/10.1021/ct3003157 | J. Chem. Theory Comput. XXXX, XXX, XXX−XXX

hydrocarbon tail and choline headgroup dynamics. Only the bond and angle parameters remain close to the standard GROMOS parameters.[28] Starting structures for DPPC and POPC bilayers were obtained from the National Center for Design of Biomimetic Nanoconductors Web site.[45] DPPC membranes contained 50 lipids in each leaflet of the membranes, while POPC membranes contained 64 lipids per leaflet. During these simulations, electrostatic interactions were truncated at 1.0 nm with interactions beyond the cutoff treated using the PME algorithm. The van der Waals interactions used a twin-range cutoff, with the short-range interactions truncated at 1.0 nm and the long-range interactions at 1.6 nm. No long-range dispersion correction was applied. Water was simulated using the SPC model.[46] In total, four simulations (two DPPC and two POPC) were performed for the GROMOS 43A1-S3 force field.

GROMOS 53A6$_L$ Force Field. The GROMOS 53A6$_L$[29,47] (or GROMOS 54A7[48]) lipid parameters use the charges of Chiu et al.,[44] with most other parameters remaining the same as in the standard GROMOS 53A6 force field.[49] The exception to this is a reparameterization of the van der Waals interactions between the methyl groups of the choline headgroup and the phosphate ester oxygen atoms. Starting structures and topologies for DPPC and POPC bilayers were obtained from the paper where these parameters were proposed,[47] and both membranes contained 64 lipids per membrane leaflet. Inspection of the POPC topology revealed that there were three $CH_2-CH_2-N-CH_3$ dihedrals in the choline headgroup, one for each of the methyl groups. However, in the GROMOS united-atom force fields, only one dihedral is applied across the same two central atoms (CH_2-N in this case). The exceptions to this are for some complex molecules (e.g., carbohydrates[50] and DNA[51]) and for repeat dihedrals with different multiplicities. In POPC, these extra dihedrals are not needed, and indeed these two additional dihedrals were not used in the simulations employed to test this force field parametrization (David Poger, personal communication). Simulations using both the downloaded POPC topology and a corrected topology were performed to evaluate the impact of these extra dihedrals on the membrane properties. Simulations performed with this force field used a twin-range cutoff for the electrostatic and van der Waals interactions. The short-range cutoff was 0.8 nm and the long-range cutoff 1.4 nm. Electrostatic interactions beyond the cutoff were treated using the reaction field (RF) method.[52] No long-range dispersion correction was applied. Water was simulated using the SPC water model with a relative dielectric permittivity constant of 62. In total, six simulations (two DPPC and four POPC) were performed for the GROMOS 53A6$_L$ force field.

Berger Force Field. The Berger lipid parameters are a combination of parameters from a variety of sources: bonded parameters are from the GROMOS87 force field[53] with Ryckaert−Bellemans dihedral parameters[54] used for the acyl chains, van der Waals parameters are from a united-atom version of the OPLS force field,[55,56] with some modifications to the acyl chain parameters by Berger and co-workers,[30] and atomic partial charges are from the calculations of Chiu et al.[44] Additionally, the original Berger parameters were extended to include unsaturated lipid tails by Tieleman and co-workers.[57−59] Topologies for the Berger lipids were obtained from the Web site of the Tieleman group.[60] However, during this work some inconsistencies with these topologies, compared to those as described by Berger et al.,[30] were discovered. First, several extraneous dihedrals were assigned in the glycerol regions of both DPPC and POPC lipid topologies, in a similar manner to those as noted for the GROMOS 53A6$_L$ POPC headgroup. Second, the van der Waals parameters for the LOS lipid ester oxygen atom type were incorrectly assigned in the parameter file (lipid.itp). The impact of these inconsistencies was evaluated through performing simulations using (i) the downloaded parameters, (ii) the parameters with the extra dihedrals removed, and (iii) the parameters with the extra dihedrals removed and corrected van der Waals parameters applied. Starting structures for the DPPC and POPC membranes were initially obtained from the Web site of the Tieleman group;[60] however, it was observed that the POPC bilayer had a different number of lipids in each leaflet of the membrane. To ensure that this uneven number of lipids did not impact upon the membrane properties, the starting structure for the GROMOS 43A1-S3 POPC simulations was also used in the Berger POPC simulations. This resulted in both DPPC and POPC membranes containing 64 lipids per leaflet of the membrane. In the original work of Berger et al., a twin-range cutoff for the electrostatic interactions (1.0/1.8 nm) was applied without any inclusion of the electrostatic interactions beyond 1.8 nm.[30] However, it has been subsequently demonstrated that this abrupt truncation of the electrostatic interactions can result in inaccurate membrane properties.[23−25] Therefore, simulations using the Berger force field were performed with a Coulombic cutoff of 1.0 nm and the long-range interactions treated using the PME method. This use of PME is the same as in most current studies that use the Berger parameters (e.g., refs 26, 61, and 62). The cutoff for the van der Waals interactions used by Berger et al. was 1.0 nm, and during the parametrization of the acyl chain van der Waals interactions, a dispersion correction beyond this cutoff was also applied.[30] While the use of a dispersion correction is most appropriately applied to isotropic systems,[63] a dispersion correction is often used in simulations of Berger lipid membranes (e.g., refs 64−66). To evaluate the impact of the dispersion correction, simulations were performed with and without this correction applied. An additional set of simulation parameters that are frequently used with the Berger lipids is a Coulombic cutoff of 0.9 nm with PME and a twin-range cutoff of 0.9 and 1.4 nm for the van der Waals interactions (e.g., refs 67−69). Simulations were also performed using these parameters to evaluate their impact upon the properties of the membranes. Water was simulated using the SPC water model in all Berger force field simulations. In total, 20 simulations (10 DPPC and 10 POPC) were performed for the Berger force field.

GROMOS 53A6 Kukol (and GROMOS-CKP) Force Field. Similarly to the GROMOS 53A6$_L$ force field, the GROMOS 53A6 lipid parameters published by Kukol[31] are an improvement of the standard GROMOS lipid parameters.[70] These lipid parameters use the charges of Chiu et al.,[44] with the majority of the other parameters being the same as those in the standard GROMOS 53A6 force field.[49] One exception to this is that the van der Waals radii of the carbonyl carbons were increased. This approach, first proposed by Chandrasekhar et al. for DPPC with the GROMOS 45A3 force field,[71] was extended to unsaturated phosphatidylcholine and phosphatidylglycerol lipids by Kukol. In addition to the modification of the carbonyl carbons, nonstandard GROMOS dihedral parameters[72] were also used for the double bond in the unsaturated lipids.[31] Lipid topologies for this force field were obtained from the original paper where the parameters were proposed[31] (with a modification to the POPC topology for use with GROMACS

dx.doi.org/10.1021/ct3003157 | J. Chem. Theory Comput. XXXX, XXX, XXX−XXX

versions 4 and above; for further details, see ref 73). Upon inspection of the POPC topology, the same extraneous dihedrals, as noted for the Berger POPC parameters previously, were found to be included here. The DPPC topology, however, did not include the additional dihedrals. Simulations of POPC membranes were performed using both the original and modified dihedral parameters. As a consequence of preliminary results, additional simulations in which the nonstandard dihedrals parameters for the unsaturated double bond were converted back into the standard GROMOS parameters (as, for example, those used in the GROMOS 53A6$_L$ POPC lipid[47]) were also performed. These POPC parameters, with the standard GROMOS double bond dihedrals, will be termed the GROMOS-CKP parameters in the remainder of the paper. It should also be noted that we have successfully applied this approach to phosphatidylethanolamine, phosphatidylglycerol, and cardiolipin membranes.[74] These GROMOS-CKP parameters are available to download from Lipidbook.[21] Starting structures for DPPC and POPC membranes were obtained from Kukol.[31] However, as for the Berger force field, the POPC membrane had a different number of lipids per leaflet. Therefore the GROMOS 43A1-S3 POPC starting bilayer configuration was also used for these simulations, resulting in both DPPC and POPC bilayers containing 64 lipids per leaflet. Simulation parameters were consistent with those used by Kukol.[31] The Coulombic interactions were truncated at 0.9 nm with interactions beyond the cutoff treated using PME. The van der Waals interactions were treated using a twin-range cutoff with the short-range interactions truncated at 0.9 nm and the long-range interactions at 1.4 nm. A long-range dispersion correction was applied to the energy and pressure. Additionally, simulations using DPPC and GROMOS-CKP POPC topologies were performed with the same simulation parameters as described for the GROMOS 53A6$_L$ force field. This was to evaluate the impact of using a standard RF treatment for the long-range electrostatic interactions with this GROMOS based force field. The SPC water model was used for all of these simulations. In total, 12 simulations (four DPPC and eight POPC) were performed for the GROMOS 53A6 Kukol and GROMOS-CKP force fields.

CHARMM36 Force Field. The all-atom CHARMM36 lipid parameter set[32] is a recent update of the widely used CHARMM27r parameters.[75] The primary improvement is that these new parameters do not require the use of a surface tension term to maintain DPPC and POPC bilayers (as well as others) in the correct liquid crystalline (Lα) phase, above the phase transition temperature.[32,76] Prior to this work, the CHARMM27 force field was available in the GROMACS package;[77] however, the CHARMM36 lipid parameter set had not been implemented. Therefore, we implemented the CHARMM36 force field in GROMACS and tested the conversion using single point simulations without cutoffs in both GROMACS[20] and NAMD.[78] The single point energies of the complete DPPC and POPC membrane systems (Tables S1 and S2) demonstrate that the force field implementation was performed with sufficient accuracy. Starting structures were obtained from the Klauda group Web site.[79] Due to the small size of the downloaded membranes (36 lipids per leaflet), additional simulations were performed with 144 lipids per leaflet to ensure that the size of the membranes did not impact the observed membrane properties. Simulation parameters replicated those as used by Klauda et al.[32] The electrostatic interactions were truncated at 1.2 nm with the interactions beyond the cutoff treated using the PME method. In contrast to the united-atom force fields, repeat simulations were not preformed through randomly assigning different starting velocities; rather the truncation of the van der Waals interactions was treated in two different ways. This was to mimic the standard protocols used in the CHARMM[80] and NAMD[78] software packages and the simulations of Klauda et al.[32] For the CHARMM approach, the van der Waals interactions were switched off between 0.8 and 1.2 nm, while for the NAMD approach the interactions were switched off between 1.1 and 1.2 nm. No long-range dispersion correction was applied. Additional simulations in which the neighbor list was extended to 1.4 nm were also performed to ensure that the truncation of the neighbor list at 1.2 nm did not impact upon the membrane properties. During the simulations, bonds to hydrogen atoms were constrained using the LINCS algorithm, and a 1 fs time step was applied. Simulations were also performed using a time step of 2 fs to evaluate the increase in the time step. Two variants of the TIP3P water model were also tested in the simulations: (i) the standard TIP3P model[81] and (ii) the CHARMM TIP3P model (also known as the TIPS3P model) that includes van der Waals interaction parameters on the water hydrogen atoms.[82,83] While the CHARMM TIP3P model was used by Klauda et al., simulations using the standard TIP3P model are quicker to perform in GROMACS and for protein systems have been suggested to have a minimal impact upon the protein dynamics.[77] Additional simulations of the DPPC membrane system were performed using the NAMD software package,[78] version 2.7b4, with both standard and CHARMM TIP3P water models. These simulations were performed to evaluate the impact of different implementations of the switching function for the truncation of the van der Waals interactions.[84] In total, 30 simulations (18 DPPC and 12 POPC) were performed for the CHARMM 36 force field.

Simulations with Optimal Parameters. In addition to the extensive series of simulations described above, a final set of 20 additional simulations were performed to allow a direct comparison of the different force fields using an optimal set of force field and simulation parameters. The same starting structures were employed for all of the force fields. All-atom DPPC and POPC membranes were obtained from the CHARMM-GUI[85] Web site.[86] Both DPPC and POPC bilayers contained 64 lipids in each leaflet of the respective membranes. These membranes were converted into appropriate starting structures for the different force fields using locally written code. Simulations were performed using the same general parameters as discussed above. The one exception to this was the CHARMM36 POPC simulations, which were performed at a temperature of 298 K to allow for a direct comparison with the united-atom POPC simulations. These comparative simulations were performed for 200 ns, and repeats, using different randomly assigned starting velocities, were performed for all of the force fields (including CHARMM36). Specific details of the optimal force field and simulation parameters chosen are discussed below:

For the GROMOS 43A1-S3 force field, only one set of force field and simulation parameters was tested, and therefore this set of parameters was also used in these simulations.

For the GROMOS 53A6$_L$ force field, the only modifications tested were in the dihedral parameters of the POPC headgroup (see above). The POPC topology with only one $CH_2-CH_2-N-CH_3$ dihedral in the choline headgroup was used in these simulations.

dx.doi.org/10.1021/ct3003157 | J. Chem. Theory Comput. XXXX, XXX, XXX−XXX

For the Berger force field, the DPPC topology selected was with the extraneous dihedrals removed, in addition to the corrected van der Waals parameters for the LOS atom type applied (see above). In contrast, the POPC topology included the extra, original dihedrals in addition to the corrected LOS van der Waals parameters. Despite the combination of corrected LOS van der Waals parameters and original dihedrals not having originally been tested, this choice was guided by the impact of removing the extra dihedrals upon the order parameters of POPC (see the Results section). These simulations used a 1.0 nm cutoff for both the Coulombic and van der Waals interactions, and a long-range dispersion correction was applied.

For the GROMOS 53A6 Kukol and GROMOS-CKP force fields, only one DPPC topology was tested. This DPPC topology and the GROMOS-CKP POPC parameters were used in these simulations. Due to the substantial increase in speed, the standard GROMOS cutoff scheme with a RF treatment for the long-range electrostatic interactions (see above for more details) was used in these simulations.

For the CHARMM36 force field, these simulations were performed using the CHARMM TIP3P water model, a cutoff of 1.2 nm for the neighbor list, switching off of the van der Waals interactions between 0.8 and 1.2 nm, and a time step of 2 fs.

Analysis. Analysis of the simulations was primarily performed through the calculation of membrane properties and a comparison of these properties to the experimentally determined values, where available (Table 2). All the calculations were averaged over the trajectories discarding the first 50 ns as an equilibration period. A block averaging analysis[87] was performed to ensure that the equilibrium membrane properties had converged. This analysis showed that for the majority of the membrane properties the standard error of the block mean converged for block sizes of ∼10−30 ns. The exception to this was for the isothermal area compressibility modulus (K_A), where for several of the simulations this property did not converge within the 200 ns simulations. A description of the methods employed to determine the membrane properties is provided below.

The average area per lipid (A_L) was calculated by simply dividing the box area in the dimension parallel to the plane of the bilayer by the number of lipids in each leaflet (n_L) and averaging the result throughout the corresponding trajectory.

The volume per lipid (V_L) was determined as

$$V_L = (V_B - V_W)/(2n_L) \quad (1)$$

where V_B is the total volume of the simulation box; V_W is the volume corresponding to a box with the same number of water molecules and at the same temperature as the target system in the absence of lipids.

The K_A was estimated considering the fluctuation of the area per molecule as

$$K_A = \frac{K_B T A_L}{n_L (sA_L)^2} \quad (2)$$

where K_B is the Boltzmann constant, T is the average temperature of the system throughout the simulation, and sA_L is the standard deviation of the A_L.

The headgroup orientation was directly determined from the average angle between the vector joining the atoms N and P and the plane of the bilayer. An angle greater than zero indicates that the headgroup is orientated above the plane of the bilayer. The calculation was done separately for each leaflet, providing identical results, within the statistical uncertainty, for all the simulations.

Deuterium order parameters were determined using locally written code for both the united-atom force fields and the all-atom CHARMM36 force field. Locally written code was used, as the GROMACS program g_order did not provide the correct order parameters for carbons in the unsaturated double bond of the POPC oleoyl tail (versions 4.0.7 and 4.5.1 of g_order were tested). For the simulations with the CHARMM36 force field, the calculation was directly obtained from the average angle between the H−C bonds and the vector perpendicular to the bilayer, since the positions of all the hydrogen atoms are explicitly known in this force field. The order parameters for simulations using the united-atom force fields involved the estimation of the hydrogen atom positions based upon an idealized geometry.

The bilayer thickness was determined from the distribution of the electron density profile of different molecular groups, namely the P atoms, the N atoms, the glycerol C atoms, and the whole lipid headgroup. The headgroup to headgroup bilayer thickness (D_{HH}) was taken as the distance between the peaks of the lipid headgroup electron density. The position of those peaks were obtained from the weighted average of the density distribution profiles corresponding to the lipid heads of each leaflet (Figure S3). The standard deviation of these peaks were used to obtain the uncertainty of the bilayer thickness by applying the propagation formula. The electron density profiles were determined using the g_density program from the GROMACS package.

Table 2. Experimentally Determined DPPC and POPC Membrane Properties[a]

membrane property	DPPC	POPC
area per lipid (nm^2)	0.629 (323 K)[104]	
	0.630 (323 K)[105]	0.630 (297 K)[108]
	0.631 (323 K)[106]	0.643 (303 K)[106]
	0.633 (323 K)[90]	0.660 (310 K)[109]
	0.640 (323 K)[89]	0.683 (303 K)[110]
	0.643 (323 K)[107]	
volume per lipid (nm^3)	1.229 (323 K)[107]	
	1.232 (323 K)[89]	1.256 (303 K)[110]
area compressibility modulus (mN/m)	231 (323 K)[89]	180−330 (298 K)[111]
bilayer thickness (nm)	3.78 (323 K)[107]	
	3.80 (323 K)[105]	
	3.83 (323 K)[89]	3.65 (303 K)[106]
	3.84 (323 K)[106]	3.70 (303 K)[110]
	3.86 (323 K)[106]	
lipid diffusion coefficient (10^{-7} cm^2/s)[b]	0.50 (313 K)[112]	
	0.70 (318 K)[113]	0.40 (303 K)[115]
	0.85 (321 K)[114]	0.89 (298 K)[116]
	0.99 (321 K)[114]	1.07 (303 K)[116]
	1.20 (321 K)[114]	1.29 (296 K)[117]

[a]The temperatures at which the experiments were performed are also provided in the table. [b]This is long-term lateral lipid diffusion, as measured through experimental techniques such as fluorescence recovery after photobleaching (FRAP) and pulsed NMR.

dx.doi.org/10.1021/ct3003157 | J. Chem. Theory Comput. XXXX, XXX, XXX−XXX

The lipid diffusion coefficients were calculated following the methodology described by Niemelä et al.[88] Briefly, the lipid displacement distribution over specific time intervals (Δt) of 2, 5, 10, 25, and 50 ns on the plane of the lipid bilayer were fitted to the equation describing the expected two-dimensional random-walk distribution:

$$P(r, \Delta t) = \frac{r}{2D\Delta t} \exp\left(-\frac{r^2}{4D\Delta t}\right) \quad (3)$$

where r is the lateral displacement and D is the lateral diffusion coefficient. The fitting was performed with our own code using a modified Newton−Raphson routine to facilitate the convergence to the minimum. The employment of this method, instead of the classical least-squares fitting of the mean square displacement to a straight line to obtain the D values from the Einstein relation, was chosen because the corresponding results do not depend upon the fitting interval.

The standard deviation was determined for all of the properties except for the area compressibility, the uncertainty of which was estimated by propagation using eq 2. The uncertainty of the diffusion coefficients is not included in the results, but it is estimated to be in the second decimal figure.

RESULTS

In this section, we will present some of the equilibrium properties of the DPPC and POPC membranes determined from simulations performed using the different force fields and simulation parameters. We will also highlight key points of comparison between force fields. The full details, for all simulations, of the electron densities, deuterium order parameters, diffusion plots, A_L, V_L, K_A, D_{HH}, diffusion coefficients, and the headgroup orientation are provided in the Supporting Information. The results below are presented separately for each force field and compared to experimental data wherever possible. At this point, it should be noted that the experimental data for these membranes is not always consistent. Differences arise due to the different experimental techniques applied and also the inherent difficulties of calculating properties, such as the A_L.[89] The experimental information provided in Table 2 is intended to provide a useful guide as to the range of the experimentally determined properties of the two membrane bilayers, at temperatures close to those used in the simulations. Finally, we also present results from simulations performed using a selected set of parameters for each force field that we consider optimal. These simulations, using the same starting structures for all force fields, allow for a direct comparison between the different force fields examined in this work.

GROMOS 43A1-S3 Force Field. This GROMOS parametrization, which includes major changes with respect to the original 43A1 force field (see the Methods section), accurately reproduces many physical properties of DPPC bilayers when compared to the available experimental data. The A_L values of 0.640 ± 0.012 nm^2 and 0.632 ± 0.014 nm^2 for the two DPPC simulations are in excellent agreement with the range of accepted experimental A_L values at the same temperature (Table 2). The V_L (1.235 ± 0.059 nm^3 and 1.235 ± 0.066 nm^3), K_A (385 ± 30 mN/m and 307 ± 27 mN/m), D_{HH} (3.46 ± 0.35 nm and 3.37 ± 0.34 nm), and lipid diffusion (10 ns: 1.707×10^{-7} cm^2 s^{-1} and 1.653×10^{-7} cm^2 s^{-1}; Tables S5, S6, and S7) are also in good agreement with experimentally determined values, although the membrane thickness is too small and the diffusion slightly too fast (Table 2). In general, the deuterium order parameters for both *sn*-1 and *sn*-2 chains are in good agreement with the experimental values. However, there is some disagreement for carbon 2 of the *sn*-2 chain, with the deuterium order parameters larger than expected (Figures S1 and S2). In the case of the POPC membranes, many of the structural and dynamic parameters also closely match the experimental data, including the A_L (0.638 ± 0.009 nm^2 and 0.638 ± 0.010 nm^2), V_L (1.252 ± 0.042 nm^3 and 1.252 ± 0.045 nm^3), K_A (482 ± 28 mN/m and 424 ± 26 mN/m), D_{HH} (3.54 ± 0.34 nm and 3.60 ± 0.34 nm; Figure 2 A), and lipid diffusion (10 ns: 0.701×10^{-7} cm^2 s^{-1} and 0.619×10^{-7} cm^2 s^{-1}; Figure 2 C and Table S7). The largest disagreement with the experimental properties is the deuterium order parameters of carbons 9, 10, and 11 of the *sn*-2 chain (Figure 2B). The order parameters of these carbon atoms, which are located next to or within the double bond of the oleoyl chain, were substantially larger (carbon 10 is ∼5 times larger) than the experimentally determined values. These results, interestingly, are in contrast to the previously published order parameters for POPC with this force field.[40] However, we believe that this difference is due to the problems associated with using the GROMACS program g_order to calculate the order parameters around the double bond (see the Methods for further details).

GROMOS 53A6$_L$ Force Field. This reparameterization of the GROMOS 53A6 force field reproduces many structural and dynamic properties of both DPPC and POPC membranes when compared to the available experimental values. For DPPC membranes, the determined equilibrium properties from the two simulations were A_L 0.629 ± 0.013 nm^2 and 0.627 ± 0.010 nm^2, V_L 1.250 ± 0.075 nm^3 and 1.249 ± 0.061 nm^3, K_A 267 ± 22 mN/m and 409 ± 27 mN/m, and D_{HH} 3.48 ± 0.36 nm and 3.55 ± 0.36 nm. For POPC, the equilibrium properties of the membranes, using the standard dihedrals (simulations L_P2a and L_P2b), were A_L 0.629 ± 0.012 nm^2 and 0.627 ± 0.009 nm^2, V_L 1.259 ± 0.070 nm^3 and 1.258 ± 0.053 nm^3, K_A 293 ± 22 mN/m and 514 ± 29 mN/m, and D_{HH} 3.63 ± 0.37 nm and 3.61 ± 0.34 nm. These are all in good agreement with the experimentally determined properties (Table 2). It is also worth noting, while still close to the experimentally determined values, that the lipid diffusion for both DPPC (10 ns: 0.898×10^{-7} cm^2 s^{-1} and 0.838×10^{-7} cm^2 s^{-1}) and POPC (10 ns: 0.383×10^{-7} cm^2 s^{-1} and 0.295×10^{-7} cm^2 s^{-1}; Table S7) was substantially slower when compared to the GROMOS 43A1-S3 force field. The largest disagreement with the experimentally determined properties was, for both DPPC and POPC membranes, in the deuterium order parameters. As previously noted by Poger et al. for DPPC,[29] the order parameters of carbons 2 and 3 of the *sn*-1 chain are too high for both lipids (Figure S2). The order parameters of carbons 9, 10, and 11 around the double bond of the *sn*-2 chain of POPC are closer to the experimental values than for the GROMOS 43A1-S3 force field (Figures S2 and 2B). As discussed in the Methods, simulations were performed using two different POPC topologies (with and without two extraneous dihedrals in the choline headgroup). Inclusion of the extra dihedrals (simulations L_P1a and L_P1b) did not substantially alter the properties of the membrane. There was a slight increase in the A_L to 0.646 ± 0.009 nm^2 and 0.634 ± 0.009 nm^2, although this is still well within the range of experimentally determined A_L. The angle the P−N vector makes with the plane of the bilayer remained the same (with one dihedral: 11.01 ± 0.06° and 11.81 ± 0.06°; with three dihedrals: 11.50 ± 0.06° and 11.59 ± 0.06°).

dx.doi.org/10.1021/ct3003157 | J. Chem. Theory Comput. XXXX, XXX, XXX−XXX

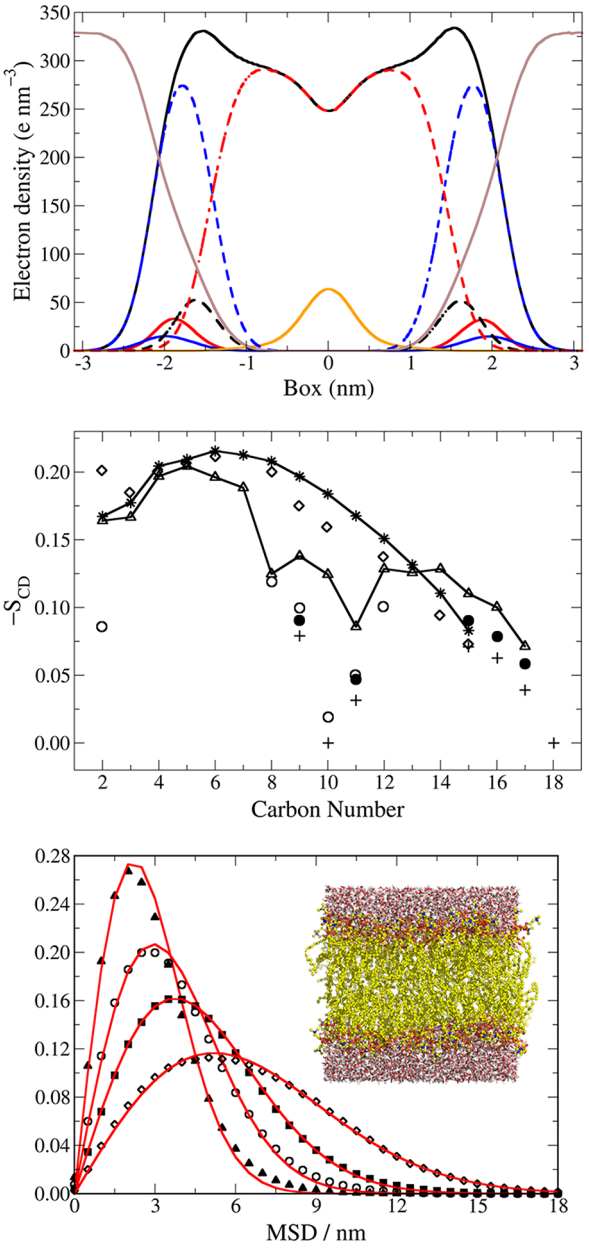

Figure 2. Results obtained from a POPC membrane simulated using the 43A1-S3 force field. TOP: Electron density profile of the P (solid red) and N (solid blue) atoms, the terminal methyl groups (solid orange), the total headgroup (dashed blue), the C atoms of the glycerol group (dashed black), the tails (dashed red), the total lipids (solid black), and the water (solid brown). CENTER: Deuterium order parameters for the *sn*-1 (*) and *sn*-2 (Δ) chains of the lipids. BOTTOM: Displacement distributions over 2 (▲), 5 (○), 10 (□), and 25 (◊) ns. Experimental deuterium order parameters are also shown in the middle plot for both chains of POPC at 300 K (◊) and (○) [Seelig et al.[91]], and only for the oleoyl chain at 296 K (●) [Warschawski and Devaux, Figure 3[92]], and at 310 K (+)[Warschawski and Devaux, Figure 2[92]]. The inset in the bottom plot is the final conformation of the simulation used for the analysis of the three panels of this figure.

Berger Force Field. As discussed in the Methods section, three different versions of the Berger force field parameters were tested: (i) the parameters as downloaded from the Tieleman group Web site,[60] (ii) these parameters with extraneous dihedrals in the glycerol region removed, and (iii) the extra dihedrals removed and modified van der Waals parameters applied for the ester oxygen atoms. These three parameter sets were tested using a van der Waals and Coulombic cutoff of 1.0 nm with PME for long-range interactions and a dispersion correction applied. The equilibrium properties of both DPPC and POPC membranes determined from simulations using parameter set i (simulations B_D1a, B_D1b, B_P1a, and B_P1b) were in decent agreement with the experimentally determined membrane properties. The A_L for DPPC was 0.675 ± 0.014 nm^2 and 0.671 ± 0.014 nm^2 and for POPC was 0.658 ± 0.013 nm^2 and 0.662 ± 0.013 nm^2. While the A_L of DPPC is ∼0.3 nm^2 greater than the accepted experimental values, the A_L of POPC is within the experimental range. The V_L for DPPC (1.195 ± 0.058 nm^3 and 1.196 ± 0.062 nm^3) and POPC (1.214 ± 0.056 nm^3 and 1.214 ± 0.056 nm^3) are both too low using this combination of force field and simulation parameters, as are the values of the D_{HH} for both DPPC (3.29 ± 0.36 nm and 3.32 ± 0.36 nm) and POPC (3.40 ± 0.35 nm and 3.50 ± 0.36 nm) membranes. The deuterium order parameters reflect the increase in A_L of DPPC and POPC compared to the GROMOS 43A1-S3 and GROMOS 53A6$_L$ force fields, with an overall decrease in order of the carbon atoms in the lipid tails (Figures 3 and S2). The largest

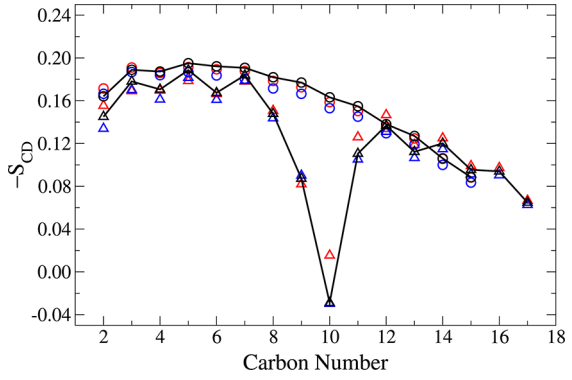

Figure 3. Deuterium order parameters obtained for the palmitoyl (circles) and oleoyl (triangles) chains of POPC calculated from three trajectories that were obtained using the original Berger force field (red). The Berger force field with the extraneous dihedrals in the glycerol region were removed (blue) and, additionally, with the van der Waals parameters of the LOS oxygen atoms were modified (black) as described in the Methods section.

disagreement with the experimentally determined deuterium order parameters is for carbon 2 in the *sn*-1 chains, with the order parameters ∼25% too low in both DPPC and POPC simulations. Removal of the extraneous dihedrals around the glycerol region of the DPPC and POPC topologies (parameter set ii) had only a minor impact upon the majority of the membrane properties. For DPPC membranes (simulations B_D2a and B_D2b), there was a slight decrease in A_L (0.666 ± 0.014 nm^2 and 0.662 ± 0.014 nm^2) and an increase in D_{HH} (3.38 ± 0.36 nm and 3.43 ± 0.37 nm). For the POPC membranes (simulations B_P2a and B_P2b), the only substantial differences were observed in the deuterium order parameters (Figure 3), in particular for carbon 10, located in the double bond of the oleoyl chain, where the deuterium order parameters were negative (∼−0.03) using the corrected topology. Modification of the ester oxygen atoms van der Waals radii (parameter set iii; simulations B_D3a, B_D3b, B_P3a, and B_P3b) did not substantially alter the deuterium order

dx.doi.org/10.1021/ct3003157 | J. Chem. Theory Comput. XXXX, XXX, XXX−XXX

parameters. These modifications did, however, reduce the A_L (DPPC: 0.650 ± 0.015 nm^2 and 0.652 ± 0.014 nm^2, POPC: 0.647 ± 0.012 nm^2 and 0.645 ± 0.012 nm^2) and increase the V_L (DPPC: 1.203 ± 0.065 nm^3 and 1.203 ± 0.061 nm^3, POPC: 1.221 ± 0.055 nm^3 and 1.221 ± 0.052 nm^3). The D_{HH} was also increased for POPC (3.57 ± 0.36 nm and 3.51 ± 0.35 nm). The resulting A_L and V_L of DPPC were closer to the experimental values. For POPC, the V_L and D_{HH} were also closer to the experimental values, with the A_L remaining within the experimentally determined range (Table 2). For all three different lipid force field parameter sets tested, the K_A, headgroup orientation, and lipid diffusion remained roughly constant and were in fairly good agreement with the experimentally determined values (Tables S5 and S7). Interestingly, the lipid diffusion was faster for both DPPC (parameter set iii 10 ns: 1.797×10^{-7} cm^2 s^{-1} and 1.864×10^{-7} cm^2 s^{-1}) and POPC (parameter set iii 10 ns: 0.844×10^{-7} cm^2 s^{-1} and 0.787×10^{-7} cm^2 s^{-1}) using these force field parameters, when compared to the GROMOS 43A1-S3 and GROMOS 53A6$_L$ force fields (Table S7). The long-term lipid diffusion coefficients for DPPC with the Berger force field using these simulation parameters are at the top of the experimentally determined range for POPC and slightly too large for DPPC (Table 2).

In addition to simulations performed with the three different Berger force field parameters, simulations were also performed using parameter set iii with two additional cutoff schemes for the van der Waals and Coulombic interactions (see the Methods for more details). Simulations were performed in which the dispersion correction for the energy and pressure was not applied (simulations B_D4a, B_D4b, B_P4a, and B_P4b), and simulations performed in which a cutoff of 0.9 nm with PME for the Coulombic interactions together with a twin cutoff of 0.9 and 1.4 nm for the van der Waals interactions were used (simulations B_D5a, B_D5b, B_P5a, and B_P5b). The removal of the dispersion correction had a substantial impact upon properties of both DPPC and POPC membranes, with an increase in the A_L, V_L, and lipid diffusion. The increase in A_L for DPPC (0.665 ± 0.013 nm^2 and 0.665 ± 0.014 nm^2) resulted in an A_L further from the experimental estimates, while the increase in A_L for POPC (0.659 ± 0.013 nm^2 and 0.653 ± 0.013 nm^2) was still within the range of experimentally determined values. The increase in V_L for both DPPC (1.265 ± 0.059 nm^3 and 1.265 ± 0.060 nm^3) and POPC (1.279 ± 0.058 nm^3 and 1.278 ± 0.058 nm^3) resulted in a V_L that was larger than the experimental values. The increase in lipid diffusion, without the dispersion correction, results in diffusion speeds for DPPC that were ∼2−3 times faster (10 ns: 2.490×10^{-7} cm^2 s^{-1} and 3.260×10^{-7} cm^2 s^{-1}; Table S7) than the upper experimental values of DPPC lipid diffusion (Table 2). The diffusion of POPC also increased (10 ns: 1.384×10^{-7} cm^2 s^{-1} and 1.265×10^{-7} cm^2 s^{-1}), although in this case to values at the upper end of the experimental range (Table 2). Simulations performed of DPPC and POPC membranes using the 0.9 nm Coulombic and 0.9/1.4 nm twin-range van der Waals cutoffs also accurately reproduced many experimental properties of these membranes. There were, however, some differences observed with these simulation parameters (compared to those described above using the initial cutoff scheme). The inclusion of the longer-range, attractive, van der Waals interactions (due to the 1.4 nm cutoff) reduced the A_L for both DPPC (0.621 ± 0.013 nm^2 and 0.619 ± 0.012 nm^2) and POPC (0.613 ± 0.011 nm^2 and 0.622 ± 0.011 nm^2) membranes. The A_L values for both membranes were slightly too low compared to the experimental values. As expected, from the reduction in A_L, there was an increase in D_{HH} for both DPPC and POPC membranes. The increase for both DPPC (3.53 ± 0.35 nm and 3.60 ± 0.36 nm) and POPC (3.67 ± 0.35 nm and 3.62 ± 0.34 nm) resulted in membrane thicknesses that remained slightly too small for DPPC but in good agreement with experimental range for POPC. The V_L also increased, when compared to simulations using the initial cutoff scheme, for both DPPC (1.220 ± 0.060 nm^3 and 1.221 ± 0.057 nm^3) and POPC membranes (1.238 ± 0.051 nm^3 and 1.238 ± 0.053 nm^3). The increases in V_L resulted in values that were closer to the experimental V_L. The use of this set of simulation parameters did not substantially impact the deuterium order parameters, with the order parameters of POPC remaining negative at carbon 10 (Figure S2).

GROMOS 53A6 Kukol (and GROMOS-CKP) Force Field. Equilibrium properties from simulations of DPPC membranes performed using the GROMOS 53A6 parameters of Kukol were in fairly good agreement with the experimentally determined membrane properties. The A_L (0.619 ± 0.009 nm^2 and 0.609 ± 0.009 nm^2) was slightly smaller than the experimental estimates and the V_L (1.259 ± 0.045 nm^3 and 1.258 ± 0.045 nm^3) slightly larger than the experimental values. The values of the D_{HH} (3.55 ± 0.36 nm and 3.68 ± 0.36 nm) were in fairly good agreement with the experimental values, although slightly too low. The deuterium order parameters were also larger for both *sn*-1 and *sn*-2 chains when compared to the experimental values (Figures S1 and S2), again in agreement with a slightly too ordered membrane. In contrast to the properties of DPPC membranes, some equilibrium properties determined from simulations of POPC membranes using the standard parameters of Kukol showed substantial disagreement with the experimentally determined membrane properties. Both the A_L (0.701 ± 0.010 nm^2 and 0.698 ± 0.008 nm^2) and V_L (1.269 ± 0.041 nm^3 and 1.269 ± 0.034 nm^3) were slightly larger than the experimentally determined properties; however, the largest differences were observed for D_{HH} and the deuterium order parameters. The observed D_{HH} of 3.27 ± 0.31 nm and 3.21 ± 0.31 nm was substantially smaller than the experimentally determined membrane thickness (Table 2). While the deuterium order parameters of the *sn*-1 palmitoyl chain were in reasonable agreement with the experimentally measured values, the deuterium order parameters for the *sn*-2 oleoyl chain substantially deviated from the experimental values (Figure 4B). In particular, the largest deviations were for carbons 11 and 12, located just after the double bond in the *sn*-2 chain, where the deuterium order parameters were negative (∼−0.05 and −0.04 for carbons 11 and 12, respectively). Simulations were also performed in which, as for the Berger force field, extraneous dihedrals in the glycerol region of the POPC topology were removed (simulations K_P2a and K_P2b; see the Methods for more details). However, unlike the Berger force field (see above), these modifications did not substantially impact the deuterium order parameters of either the *sn*-1 or *sn*-2 chains. The modifications did, however, impact A_L, V_L, and D_{HH} for this force field (Figure 4). Removal of the extraneous dihedrals reduced the A_L (0.669 ± 0.009 nm^2 and 0.661 ± 0.011 nm^2; Figure 4A) and increased the D_{HH} (3.42 ± 0.31 nm and 3.53 ± 0.32 nm). The resulting A_L was within the experimental range, and D_{HH} improved compared to the experimental value for POPC. The increased order of the membrane was also reflected in the deuterium order parameters, with a general overall increase in the order

dx.doi.org/10.1021/ct3003157 | J. Chem. Theory Comput. XXXX, XXX, XXX−XXX

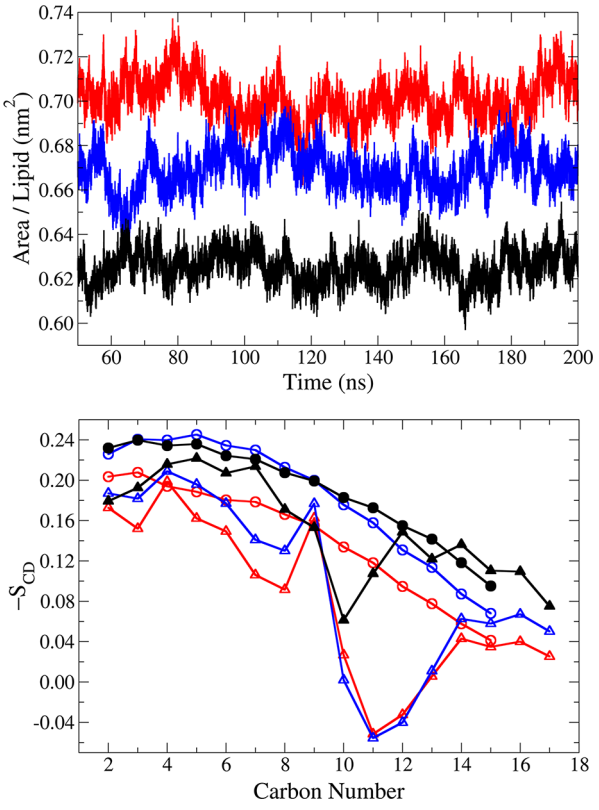

Figure 4. Area per lipid (top) and deuterium order parameters (bottom) for the palmitoyl (circles) and for the oleoyl (triangles) of three POPC bilayers that were obtained using the original GROMOS53A6 Kukol force field (red), the same force field but without the extraneous dihedrals in the glycerol region (blue), and with the GROMOS-CKP parameters (black).

parameters for both *sn*-1 and *sn*-2 chains, apart from carbons 9−11 of the *sn*-2 chain. As mentioned above, the overall trends in the order parameters were not substantially altered (Figure 4B). The removal of the extraneous dihedrals increased the V_L (1.280 ± 0.041 nm^3 and 1.278 ± 0.050 nm^3), such that the V_L was further from the experimental value. In addition to the corrected dihedrals, simulations were performed with the nonstandard dihedral parameters for the double bond converted back to the standard GROMOS parameters (simulations K_P3a and K_P3b). Simulations performed using these GROMOS-CKP parameters led to a further reduction in the A_L (0.625 ± 0.007 nm^2 and 0.627 ± 0.008 nm^2) and a further increase in D_{HH} (3.65 ± 0.34 nm and 3.64 ± 0.36 nm). This resulted in an A_L slightly smaller than the lower experimental values (Figure 4A). The increase in D_{HH} resulted in a membrane thickness in good agreement with the experimentally determined values. Additionally, there was a decrease in V_L (1.274 ± 0.035 nm^3 and 1.275 ± 0.037 nm^3), toward the experimental value for the POPC. The most dramatic impact of the modified double bond dihedral parameters was in the deuterium order parameters (Figure 4B). As expected, given the decrease in A_L, there was an overall increase in the order parameters of both chains. However, the largest change in the order parameters of the *sn*-2 chain was within the vicinity of the double bond (carbons 5−8 and 10−16). The modifications to the double bond dihedrals resulted in a substantial improvement in the deuterium order parameters, reaching good agreement with the experimental values (Figures 2B and 4B). The diffusion of both DPPC and POPC was the slowest of all force fields tested in this work, with the diffusion close to or slightly slower than the experimental range of diffusion (DPPC 10 ns: 0.644 × 10^{-7} cm^2 s^{-1} and 0.585 × 10^{-7} cm^2 s^{-1}; POPC 10 ns: 0.287 × 10^{-7} cm^2 s^{-1} and 0.279 × 10^{-7} cm^2 s^{-1}; Table S7). Additionally, the values for the K_A were slightly higher than the other force fields, although this membrane property was generally quite variable between repeat simulations (Table S5). For both the standard DPPC and the GROMOS-CKP POPC force field parameters, additional simulations were performed using a standard GROMOS cutoff scheme and a RF correction applied for the long-range electrostatic interactions (simulations K_D2a, K_D2b, K_P4a, and K_P4b). This cutoff scheme did not substantially impact the membrane properties, with a slight increase in A_L (DPPC: 0.622 ± 0.010 nm^2 and 0.626 ± 0.010 nm^2; POPC: 0.630 ± 0.010 nm^2 and 0.639 ± 0.007 nm^2) and lipid diffusion (DPPC 10 ns: 0.796 × 10^{-7} cm^2 s^{-1} and 0.637 × 10^{-7} cm^2 s^{-1}; POPC 10 ns: 0.421 × 10^{-7} cm^2 s^{-1} and 0.340 × 10^{-7} cm^2 s^{-1}; Table S7) toward the experimental ranges of values. However, there was also an increase in V_L (DPPC: 1.277 ± 0.048 nm^3 and 1.277 ± 0.046 nm^3; POPC: 1.292 ± 0.049 nm^3 and 1.292 ± 0.034 nm^3), to values further from the experimentally determined V_L.

CHARMM36 Force Field. The recently published CHARMM36 force field was the only all-atom force field examined in the present work. Several factors were investigated for each of the two lipids: the water model, the time step, the bilayer size, and the neighbor list cutoff. For each combination of parameters, the distance for switching off the van der Waals interactions was set between 0.8 and 1.2 nm and also between 1.1 and 1.2 nm, labeled as simulations 'a' and 'b' from now on (see the Methods for more details). Simulations performed of DPPC and POPC membranes with the CHARMM TIP3P water accurately reproduced many of the experimental properties of these membranes. In particular, for the deuterium order parameters of both DPPC and POPC, this was the only force field tested that accurately reproduced the experimental order parameters of carbon 2 from both *sn*-1 and *sn*-2 chains in DPPC and POPC (Figure 5C). The other order parameters were also in good agreement with the experimental values, including the characteristic drop in order for the double bond in the oleoyl tail of POPC. Apart from the deuterium order parameters, other properties of the membranes are reasonably well reproduced. The A_L was too low for DPPC simulations (a: 0.591 ± 0.017 nm^2 and b: 0.588 ± 0.016 nm^2), although the A_L from the POPC simulations (a: 0.635 ± 0.017 nm^2 and b: 0.630 ± 0.021 nm^2) was within the experimental range. The D_{HH} was also slightly too large for DPPC (a: 3.97 ± 0.39 nm and b: 3.85 ± 0.38 nm) and in good agreement with the experimental values for POPC (a: 3.69 ± 0.37 nm and b: 3.74 ± 0.37 nm) membranes. The V_L was slightly too low for both DPPC (a: 1.198 ± 0.085 nm^3 and b: 1.190 ± 0.079 nm^3) and POPC (a: 1.221 ± 0.082 nm^3 and b: 1.213 ± 0.098 nm^3) membranes. The diffusion of both lipids (e.g., DPPC 10 ns: 2.681 × 10^{-7} cm^2 s^{-1}; POPC 10 ns: 1.238 × 10^{-7} cm^2 s^{-1} for simulations C_D3a and C_P3a, respectively) was faster than with the three GROMOS force field parametrizations, and the diffusion of POPC was also faster than the Berger force field (apart from the Berger simulations B_P4a and B_P4b, which used the 1.0 nm cutoff without a dispersion correction; Table S7). The POPC diffusion coefficient was within the experimental range, while the DPPC diffusion was dependent upon the van der Waals

dx.doi.org/10.1021/ct3003157 | J. Chem. Theory Comput. XXXX, XXX, XXX−XXX

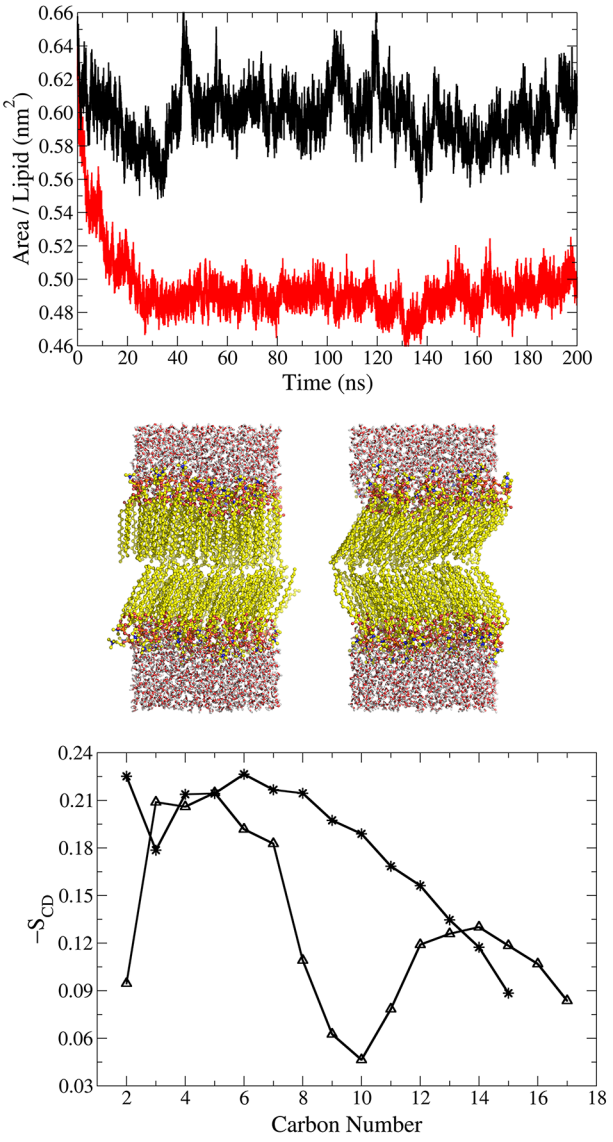

Figure 5. Area per lipid for DPPC (red) and POPC (black) bilayers that were simulated using the CHARMM36 force field with the standard TIP3P water model (top). Two images of a DPPC bilayer in the gel phase corresponding to the final configuration of the same DPPC simulation shown in the top panel (center). Deuterium order parameters of the palmitoyl (*) and oleoyl (▲) chains of a POPC bilayer simulated using the CHARMM36 force field with the CHARMM TIP3P water model (bottom).

switching distance (see below). The average angle the P−N vector in the choline headgroup made with the plane of the bilayer during the DPPC simulations (a: 16.63 ± 0.06° and b: 16.78 ± 0.06°) and POPC (a: 18.49 ± 0.06° and b: 18.46 ± 0.06°) was larger than for any of the united-atom force fields. While the increase in time step, system size, and extension of the neighbor list had relatively little impact upon the properties of the membranes (see the Supporting Information), the point at which the van der Waals interactions were switched off (0.8 or 1.1 nm) had a greater impact. Inclusion of the full van der Waals interactions to 1.1 nm slightly decreased both the A_L and the V_L (see the values given above), resulting in a more ordered membrane. This distance at which the van der Waals interactions were switched off also impacted the diffusion of the DPPC lipids, as did the increase in bilayer size. The diffusion with the 0.8 nm switching distance was generally faster than with the 1.1 nm switching distance (e.g., 0.8 nm 10 ns: 2.681×10^{-7} cm^2 s^{-1}; 1.1 nm 10 ns: 2.177×10^{-7} cm^2 s^{-1} for simulations C_D3a and C_D3b, respectively; Table S7) and was also above the experimental range for the diffusion of DPPC. The increase in system size reduced the diffusion of DPPC by ∼30% (e.g., 10 ns: 2.177×10^{-7} cm^2 s^{-1}; 10 ns: 1.414×10^{-7} cm^2 s^{-1} for simulations C_D3b and C_D6b, respectively), although the impact upon the diffusion of POPC was less obvious (Table S7). The simulation parameter that had the largest influence upon the membrane properties was the choice of TIP3P water model. DPPC simulations using the standard TIP3P water underwent a transition to a tilted gel phase within the first 50 ns of the simulations (Figure 5A and B). This transition was independent of the two neighbor list cutoffs tested but was dependent upon the point at which the switching off of the van der Waals interactions occurred. The phase transition only occurred with the switching at 1.1 nm. This cutoff dependent phase transition is highlighted by the A_L (C_D1a: 0.563 ± 0.017 nm^2 and C_D1b: 0.490 ± 0.009 nm^2), D_{HH} (C_D1a: 3.99 ± 0.38 nm and C_D1b: 4.15 ± 0.35 nm), deuterium order parameters (Figure S2), and electron density profiles (Figure S3). To further probe the cause of the transition to the gel phase, we performed a series of simulations using the NAMD software (Table S3). These DPPC simulations were performed using both the standard TIP3P and the CHARMM TIP3P water models and with different methods for the truncation of the van der Waals interactions at 1.1 nm (either the potential energies or the forces were switched off at this point). While the switching of the energies is the method by which the truncation of the interactions occurs in GROMACS, the recommended option in CHARMM is to switch off the forces. The A_L from the simulations performed in NAMD demonstrated that the transition to the gel phase occurred due to a combination of the standard TIP3P water model and the switching off of the energy. The transition did not occur with the standard TIP3P model and a switching off of the forces (Table S3). The standard TIP3P water model had a less dramatic impact upon the properties of the POPC membranes. There was an ordering of the membrane with a reduction in the A_L (C_P1a: 0.604 ± 0.014 nm^2 and C_P1b: 0.598 ± 0.014 nm^2) and an increase in D_{HH} (C_P1a: 3.84 ± 0.37 nm and C_P1b: 3.77 ± 0.36 nm). However, this ordering was not to the same extent as for DPPC, and the standard TIP3P model did not induce a phase transition with POPC.

Simulations with Optimal Parameters. As discussed in the Methods, additional simulations were also performed using what we believe to be an optimal set of parameters for each force field. The results in this section are presented for all of the studied force fields together, to allow for an easier comparison between them. The main results obtained from these simulations are summarized in Table 3 and Figure 6, with all of the results additionally provided in the Supporting Information. It should also be noted that they are, in general, in excellent agreement with the simulations discussed above, when using the same simulation and force field parameters (although with different starting structures). Furthermore, the membrane properties determined from these simulations in general were also in excellent agreement with those previously reported using these (or very similar) force field and simulation parameters (where available; e.g., refs 23−25, 28−32, 47).

dx.doi.org/10.1021/ct3003157 | J. Chem. Theory Comput. XXXX, XXX, XXX−XXX

Table 3. A_L, V_L, K_A, D_{HH}, the Angle between the Bilayer Surface and the Vector Joining the P−N Atoms, and the Lipid Diffusion Coefficients Obtained from the MSD Distributions at 10 ns of the DPPC and POPC Lipids for the Simulations Using the Optimal Parameters for Each Force Field (See the Methods for Further Details)[a]

lipid	force field	A_L (nm^2)	V_L (nm^3)	K_A (mN·m^{-1})	P−N angle (degrees)	D_{HH} (nm)	diffusion coefficient (10^{-7} cm^2 s^{-1})	performance (ns/day)[b]	system size (particles)
DPPC	43A1-S3	0.640 ± 0.012	1.232 ± 0.053	338 ± 25	9.17 ± 0.06	3.52 ± 0.36	1.336	45.46	17,377
		0.636 ± 0.012	1.232 ± 0.056	299 ± 23	9.01 ± 0.05	3.51 ± 0.36	1.124	44.11	17,377
	53A6$_L$	0.631 ± 0.011	1.231 ± 0.050	379 ± 26	9.01 ± 0.06	3.46 ± 0.36	0.913	179.68	17,377
		0.623 ± 0.013	1.230 ± 0.061	262 ± 22	8.82 ± 0.06	3.52 ± 0.36	0.964	181.07	17,377
	Berger	0.652 ± 0.014	1.203 ± 0.062	233 ± 20	9.23 ± 0.04	3.49 ± 0.37	1.842	51.12	17,377
		0.652 ± 0.014	1.203 ± 0.062	238 ± 20	9.18 ± 0.04	3.40 ± 0.36	1.898	55.79	17,377
	53A6 Kukol	0.622 ± 0.009	1.277 ± 0.044	523 ± 31	7.37 ± 0.04	3.60 ± 0.38	0.678	188.33	17,377
		0.620 ± 0.010	1.278 ± 0.047	454 ± 29	7.21 ± 0.06	3.52 ± 0.38	0.663	170.54	17,377
	CHARMM36	0.586 ± 0.015	1.192 ± 0.074	182 ± 19	16.62 ± 0.04	3.73 ± 0.39	1.835	23.77	27,617
		0.594 ± 0.014	1.195 ± 0.069	210 ± 20	16.73 ± 0.04	3.77 ± 0.39	1.683	23.62	27,617
POPC	43A1-S3	0.639 ± 0.011	1.254 ± 0.051	366 ± 25	10.98 ± 0.05	3.51 ± 0.34	0.653	42.49	18,776
		0.638 ± 0.011	1.254 ± 0.052	358 ± 24	10.31 ± 0.04	3.65 ± 0.35	0.647	41.93	18,776
	53A6$_L$	0.633 ± 0.010	1.248 ± 0.049	408 ± 26	11.05 ± 0.06	3.64 ± 0.37	0.379	165.94	18,776
		0.633 ± 0.010	1.248 ± 0.050	385 ± 25	11.10 ± 0.06	3.53 ± 0.35	0.480	169.37	18,776
	Berger	0.651 ± 0.014	1.224 ± 0.066	209 ± 19	12.15 ± 0.04	3.47 ± 0.36	0.803	53.62	18,776
		0.643 ± 0.014	1.224 ± 0.065	219 ± 19	12.12 ± 0.05	3.53 ± 0.36	0.632	53.53	18,776
	CKP	0.635 ± 0.008	1.295 ± 0.039	639 ± 32	9.80 ± 0.04	3.53 ± 0.36	0.414	177.98	18,776
		0.627 ± 0.009	1.294 ± 0.044	523 ± 29	8.72 ± 0.05	3.70 ± 0.37	0.312	163.02	18,776
	CHARMM36	0.630 ± 0.014	1.211 ± 0.067	210 ± 19	18.66 ± 0.04	3.76 ± 0.38	0.988	23.28	29,272
		0.629 ± 0.012	1.210 ± 0.059	269 ± 21	18.71 ± 0.04	3.69 ± 0.38	1.113	23.08	29,272

[a]Systems sizes and simulation performances are also provided in this table. [b]All simulations were performed using six 2.4 GHz Intel Westmere 12-core nodes (so 72 cores in total) on the University of Southampton Iridis 3 machine. We note that no optimization of the PME settings was attempted for the simulations in which PME was used, rather the same number of separate PME nodes was used in all united-atom DPPC and in all united-atom POPC simulations. Further improvements in performance are likely to be achieved through an optimization of these settings, for example, using the GROMACS tool g_tune_pme.

A combination of the A_L, K_A, D_{HH} (Table 3), and deuterium order parameters (Figure 6) indicate the degree of ordering and elasticity of the membranes during these simulations. For DPPC, simulations performed using the CHARMM36 force field resulted in the most ordered membranes, followed by the GROMOS 53A6 Kukol, GROMOS 53A6$_L$, and GROMOS 43A1-S3 force fields; the most disordered DPPC membrane resulted from using the Berger force field. While the A_L of the DPPC membranes simulated using the GROMOS 53A6$_L$, GROMOS 43A1-S3, and Berger force fields were within the experimental range, the D_{HH} values of the membranes using these force fields were too low (Table 3). In contrast, the A_L values of the membranes using the CHARMM36 and GROMOS 53A6 Kukol were slightly too low (more so for the CHARMM36 force field); however, the values of D_{HH} were closer to the experimental values for the membrane thickness. Similar trends in membrane order were observed for the POPC simulations, although the properties of the CHARMM36 POPC membrane were closer to the properties of the membranes simulated using the united-atom force fields (Table 3). The greatest elasticities of both DPPC and POPC membranes were observed with the CHARMM36 force field, followed by the Berger, GROMOS 53A6$_L$, and GROMOS 43A1-S3 force fields. The GROMOS 53A6 Kukol/GROMOS-CKP force fields had the lowest elasticity, with the largest K_A and smallest standard deviation in the A_L.

In addition to providing an indication of the overall ordering of the lipid tails within the membrane, the deuterium order parameters also provide further details regarding the local structure and conformation of regions of the lipid tails in the simulations. Between force fields, there were two parts of the deuterium order parameters where substantial differences were observed (Figure 6). The first of these was for carbon 2, a carbon atom located close to the glycerol group of the lipid, and was observed in both the DPPC and POPC simulations. Experimentally there is an observed difference in ordering of this carbon between the *sn*-1 and *sn*-2 tails of the lipid, with a lower order parameter of the *sn*-2 tail at this point[90,91] (Figures 2B and S1). The GROMOS 53A6$_L$ and GROMOS 53A6 Kukol/GROMOS-CKP force fields were in fairly good agreement for the ordering of this carbon; however, the closest agreement was with the all-atom CHARMM36 force field (Figure 6). Furthermore, the CHARMM36 force field was also in closer agreement with the experimental values for carbons 3 and 4 in both tails. The second area of difference was for the carbon atoms located within (9 and 10) or next to (8 and 11) the double bond in the oleoyl tail of the POPC lipids. Experimentally there is a characteristic drop in the deuterium order parameter for carbon 10 of the oleoyl tails.[91,92] This drop in the deuterium order parameter at carbon 10 was reasonably well reproduced for all of the force fields apart from the GROMOS 43A1-S3 force field (Figure 6). For this force field, there were lower order parameters for carbons 8 and 11, with slightly higher order parameters for carbons 9 and 10. Slight differences in the deuterium order parameters for these carbons with the other force fields were also observed. In particular, the size of the order parameter for carbon 10 differed between force fields. The smallest value was with the Berger force field (to ∼0.01), with the largest for the GROMOS 53A6$_L$ and GROMOS 53A6 Kukol/GROMOS-CKP force fields (to

dx.doi.org/10.1021/ct3003157 | J. Chem. Theory Comput. XXXX, XXX, XXX−XXX

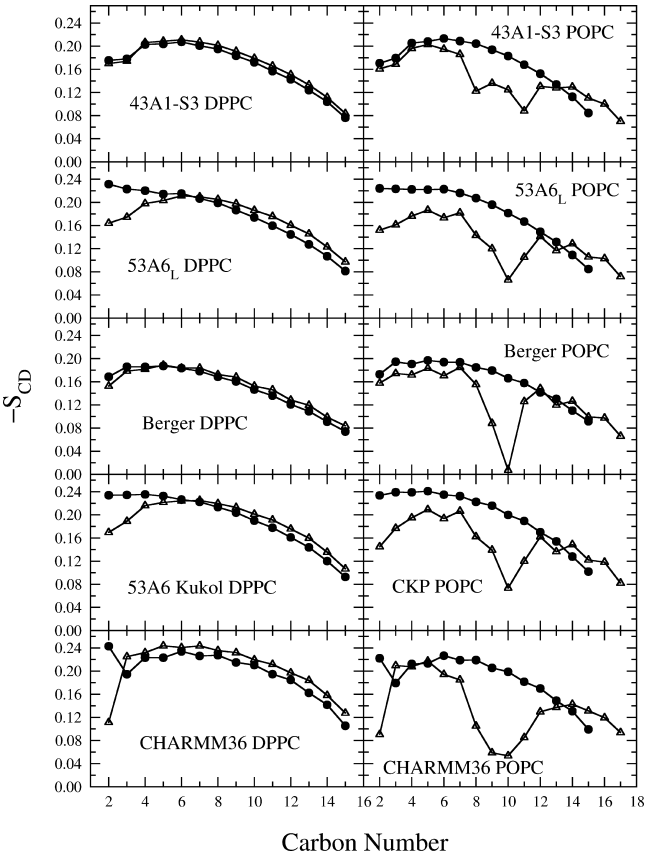

Figure 6. Deuterium order parameters obtained for the *sn*-1 (*) and *sn*-2 (Δ) chains of the lipids from one of the replicas of the simulations with optimal parameters for the five force fields.

~0.06). The CHARMM36 and Berger force fields were closer to the experimentally determined values for the deuterium order parameter of this carbon[91,92] (Figure 2B). Further details regarding the conformation of the lipids can be determined from the angle that the P−N vector in the lipid headgroup makes with the plane of the membrane. In general, all of force fields were in good agreement with the experimental observation that the headgroup lies roughly parallel to the plane of the membrane.[93] There were, however, some differences between force fields, with a slightly more perpendicular orientation (~ 5−10°) observed in the CHARMM36 membranes when compared to the united-atom force fields (Table 3).

The diffusion of the lipids within the membrane is another important membrane property. Indeed, despite the fairly large range of experimental values that have been reported, it is frequently used in the validation of lipid force fields (e.g., refs 71 and 94). Substantial differences between the force fields studied in this work were observed for the diffusion coefficients. The fastest diffusion using the optimal simulation parameters was for the CHARMM36 force field, followed by the Berger, GROMOS 43A1-S3, GROMOS 53A6$_L$, and finally GROMOS 53A6 Kukol/GROMOS-CKP (Table 3). For DPPC membranes, the diffusion coefficients determined for the CHARMM36 and Berger simulations were slightly larger than the range of experimental properties shown in Table 2. The diffusion of DPPC in the other united-atom force fields was within the range of experimentally determined values. In contrast, for the POPC simulations, the GROMOS 53A6$_L$ and GROMOS-CKP simulations were at and slightly below the lower end of the experimental range. The other POPC force fields were within the experimentally determined range of the POPC diffusion (Table 2).

DISCUSSION

Several lipid force field and simulation parametrizations were assessed in the present work for both DPPC and POPC lipid bilayers. Our analysis has demonstrated that the bilayer structure and the dynamics of the lipids can be sensitive to specific changes in the force field parameters and in the simulation conditions.

The Berger force field is one example where both force field and simulation parameters were observed to influence the membrane properties. Modifications of the initial topologies to remove extraneous dihedrals and to correct the ester oxygen atoms' van der Waals radii resulted in an increase in order for both DPPC and POPC membranes. The removal of the additional dihedrals had further consequences for the deuterium order parameters of the lipids in the POPC membranes. Removal of the dihedrals in the glycerol region resulted in a negative order parameter for carbon 10, located in the double bond of the oleoyl chain. This, somewhat unexpected, impact meant that the order parameters for this carbon atom were further away from the experimental values. Interestingly, for POPC, it would seem that these additional dihedrals, initially considered extraneous based upon standard GROMOS force field bonded parameters, improve some properties of the POPC membranes, and therefore we recommend their use. In the case of DPPC, the same dihedrals do not substantially modify the behavior of the order parameters. Three different sets of commonly used simulation parameters were also tested for the Berger force field, with different treatments for the truncation of the van der Waals producing the largest impact upon the properties of the membrane. The initial cutoff scheme used a 1.0 nm van der Waals cutoff and a long-range dispersion correction. Removal of the dispersion correction decreased the order of both the DPPC and POPC membrane (as exemplified by the increase in A_L) and substantially increased the lipid diffusion. Presumably the removal of the attractive long-range interactions decreased the interlipid tail interactions and therefore increased the membrane disorder and lipid diffusion rate. Without this dispersion correction, the diffusion of DPPC was faster than the experimentally determined diffusion rates. Including some of the attractive long-range van der Waals, with the third cutoff scheme tested (twin range 0.9/1.4 van der Waals cutoff), increased the order in the membrane and reduced the lipid diffusion. The results from these three simulations highlight the impact that the choice of simulation cutoffs can have upon the membrane properties. In particular, for the choice of simulation parameters to use with this force field, we recommend avoiding the 1.0 nm cutoff without a dispersion correction for DPPC membranes, as both the lipid diffusion and V_L are in greatest disagreement with the experimentally determined range of values. We do, however, note that the increase in lipid diffusion may be desirable in some situations due to an increase in sampling. The inclusion of the dispersion correction generally improves the agreement with the experimental values. Use of a 0.9/1.4 twin-range cutoff for the van der Waals interactions further improved some membrane properties (e.g., D_{HH}), although it resulted in the greatest disagreement with experimental values for other membrane properties (e.g., A_L).

dx.doi.org/10.1021/ct3003157 | J. Chem. Theory Comput. XXXX, XXX, XXX−XXX

Therefore we see no substantial benefit from using this set of simulation parameters, especially given the increase in simulation time. A compromise between sets of simulation parameters (such as a 0.9/1.2 nm twin-range cutoff) may in fact be the optimal set of simulation parameters to use for DPPC with this force field. However, of the three simulation parameter sets explicitly tested in this study, we would recommend the use of a 1.0 nm cutoff with a dispersion correction.

Another example where the choice of parameters can have a large impact upon the membrane properties is the CHARMM36 force field. The use of the standard TIP3P water model, in conjunction with certain treatments for the switching off of the van der Waals interactions, induced a transition in DPPC membranes to a tilted gel phase. A similar impact of the standard TIP3P model has been previously observed for a 1,2-dioleoyl-*sn*-glycero-3-phosphocholine (DOPC) membrane simulated using the CHARMM27 force field.[95] The exact mechanisms underlying the reduction in A_L are not completely clear. However, as noted previously,[76,95] the lateral organization of lipids in the membrane is highly sensitive to the bulk water properties due to both water−lipid and lipid−lipid nonbonded interactions. While the use of the 1.1 nm switching distance for the van der Waals interactions is required for the phase transition to occur, the use of this cutoff also decreased the A_L for both DPPC and POPC when the membranes were simulated using the CHARMM TIP3P water model. This increase in order of the membranes is presumably due to inclusion of a greater number of attractive van der Waals interactions with the longer distance at which to start switching off the van der Waals interactions. These simulations also indicate, in agreement with Klauda et al.,[32] that any longer van der Waals cutoffs with this force field would not be an appropriate choice. We also, therefore, recommend the use of the 0.8 nm van der Waals switching distance with the CHARMM TIP3P water when simulating lipid membranes using this force field within GROMACS. The recommendation of CHARMM TIP3P water model is in contrast to previous work performed for protein simulations with the CHARMM27 force field in GROMACS, which reported only a minimal impact of the choice of TIP3P model upon the protein dynamics.[77] Therefore, in contrast to this previous work, we have shown that it would be desirable to implement the optimized water loops for CHARMM TIP3P in GROMACS. Additionally, it would also be desirable to implement the CHARMM force switching method for the truncation of the van der Waals interactions,[84] although we have shown this not to be essential for DPPC and POPC membrane simulations with this force field.

However, not all of the changes in simulation parameters tested in this work had a substantial impact upon the membrane properties. Notably, for the CHARMM36 force field, an increase in time step to 2 fs did not substantially impact the membrane properties. The increase in time step is important, as this is one of the key factors that determines the speed of the simulations. We have shown that there are no substantial differences in the membrane properties between simulations performed with a 1 and 2 fs time step, and so we recommend the use of a 2 fs time step. Given this result, it would also be of interest in the future to examine the use of larger (e.g., 4 fs) time steps with the united-atom force fields. The increase in system size with the CHARMM36 force field also did not have a substantial impact upon the majority of the properties of the membranes. This observation is in agreement with previous studies looking at the impact of system size upon simulated membrane properties.[96−98] The one exception to this was for the diffusion of DPPC, where there was a reduction in the lipid diffusion rate with an increase in system size, again in agreement with previous work.[98] Presumably this was due to a reduction in the correlated motions of the lipids across the periodic boundaries in the larger system. The general lack of impact of the size of the system is also important, as this provides confidence that the properties observed from the simulations presented in this work, using fairly small membranes, will be consistent with the membrane properties of larger systems. The change in simulation parameters with the GROMOS 53A6 Kukol DPPC and GROMOS-CKP POPC membranes to use a standard GROMOS cutoff did not substantially impact the membrane properties. This is also interesting as simulations performed using this cutoff scheme were ∼3 times faster to perform than with the original cutoff scheme of Kukol (primarily due to the use of RF instead of PME, as has been observed previously with simulations using the Berger force field[27]). Indeed, due to this substantial increase in performance using the standard GROMOS cutoff scheme, we would recommend using this set of cutoffs when simulating DPPC and POPC membranes with these parameters. If the use of PME is desired for the simulation, as for example may be the case when simulating membrane and protein systems,[99] the original cutoff scheme of Kukol can be used without a substantial impact upon the membrane properties.

Four out of the five force fields tested were able to fairly accurately reproduce many experimental properties of both DPPC and POPC membranes, given appropriate simulation parameters. The one exception was the GROMOS 53A6 POPC parameters of Kukol, where the standard parameters showed substantial disagreement with the experimental values for several membrane properties. The biggest differences were for the membrane thickness (D_{HH}) and deuterium order parameters. Due to these substantial differences between simulation and experiment, we suggest that these parameters should not be used for simulating POPC membranes. Removal of the extraneous dihedrals and conversion of the double bond parameters into the standard GROMOS parameters improved the properties of POPC membranes. These new parameters (the GROMOS-CKP parameters), which were in agreement with many of the experimental POPC membrane properties, have also been further developed to other classes of phospholipids.[74]

Most of the force fields studied in this work accurately reproduced most of the available experimental data, given appropriate force field and simulation parameters. However, as highlighted in the simulations with the optimal parameters, there were still some interesting differences that were observed between force fields.

The most striking differences arose in the diffusion of the lipids. While there was some intra-force-field dependence upon the simulation parameters used, the general trends in diffusion were that the fastest diffusion was with the Berger and CHARMM36 force fields, followed by the GROMOS 43A1-S3 force field and GROMOS 53A6$_L$ force field, and finally the slowest diffusion was with the GROMOS 53A6 Kukol/GROMOS-CKP force field. Most of the diffusion speeds for both DPPC and POPC were within or close to the experimental range of values. The reasons for the observed differences in diffusion arise from a combination of the different

simulation parameters and different force field parameters used in the simulations. The impact of the simulation parameters upon the lipid diffusion is highlighted in the Berger force field, where the inclusion of some of the longer range van der Waals interactions (either through a dispersion correction or an increase in cutoff) leads to a substantial reduction in lipid diffusion. The impact of the force field parameters can be highlighted from a comparison of the GROMOS 53A6 Kukol/GROMOS-CKP force fields with the Berger force field. In these two force fields, the partial charges of the lipids are the same, as are the majority of the bonded interaction parameters. The differences are primarily in the Lennard-Jones parameters for the van der Waals interactions, with differences also in the dihedral parameters for the lipid tails. These differences give rise to substantially different lipid diffusion rates for these force fields. This also indicates how modifications may be made to some of the force fields to improve the lipid diffusion. For example, we anticipate that with modifications to the van der Waals parameters for the lipid tails in the GROMOS 53A6 Kukol/GROMOS-CKP force fields, the lipid diffusion rates could be increased. Interestingly, observed differences in rates of diffusion can provide an explanation for some previously reported observations. Poger et al.[29] noted that the self-assembly of a DPPC membrane performed using the GROMOS $53A6_L$ force field took substantially longer than self-assembly simulations performed by Marrink et al. of a DPPC membrane using the Berger force field.[100] The differences observed in the rates of diffusion of these lipids, especially given the direct 1.0 nm van der Waals cutoff used by Marrink et al.,[100] explain the differences observed in the time scales of the self-assembly process and in particular differences in the slow membrane resealing in the final stage of self-assembly. This example highlights how an increase in sampling with a faster diffusing lipid may be advantageous. Indeed, this increase in diffusion may guide the combination of parameters when attempting to observe longer time scale membrane events using atomistic MD simulations. However, the choice of parameters should not only be based upon the diffusion rates but also combined with the efficiency of performing the simulations (Table 3). For example, the increase in simulation efficiency using a RF cutoff may offset the slower diffusion using the GROMOS $53A6_L$ and GROMOS 53A6 Kukol/GROMOS-CKP force fields. Similarly, the increase in diffusion with the CHARMM36 force field may also offset some of the associated costs in using an all-atom force field (Table 3). Therefore, if the goal is to achieve maximal sampling, the Berger force field should be used due for the combination of fast diffusion and good simulation efficiency. We should also note that the use of the Berger force field with a RF cutoff has been tested previously (e.g., refs 23, 25, and 27) and this should further maximize the sampling efficiency, although we stress that the validity of this combination of simulation and force field parameters was not tested in this work.

Another area where there were interesting differences between force fields was for the deuterium order parameters of the lipid tails. The all-atom CHARMM36 force field was generally in closest agreement with the experimentally determined values. For POPC membranes and the GROMOS 43A1-S3 force field, the deuterium order parameters of the carbons in the double bond of the oleoyl chain were in substantial disagreement with the experimentally determined values. Therefore, despite the other properties of the membrane being in a good agreement with the experimentally determined values, we would recommend caution in using this force field when simulating POPC membranes.

In addition to highlighting any simulation and force field parameters that we would recommend to use or not use, it is interesting to reflect upon the different membrane properties analyzed from the simulations. Differences in lipid diffusion, as highlighted above, can be quite substantial between force fields. However, there are also large variations in the experimentally determined values for the lipid diffusion. This makes this property difficult to use when purely looking at the accuracy of the simulations. The same is true for several other membrane properties including A_L and K_A. Indeed, determining the K_A from the simulations can also suffer from problems of insufficient sampling, even with these fairly long 200 ns simulations, as the K_A is determined using the variance of the A_L. This problem is highlighted in the variability of the values of the K_A from the repeat simulations (Tables 3 and S5). For the other determined membrane properties, we have observed that the D_{HH} is generally in disagreement with the A_L; when the values of the D_{HH} are in close agreement with the experimental range, the A_L is too low (and *vice versa*). This is perhaps due to the issues of determining these properties experimentally. Additionally, as discussed above, we have observed that the deuterium order parameters of the lipid tails are quite variable between force fields; these are areas where improvements to some of the force fields can be made in the future.

CONCLUSIONS

In conclusion, we have studied the ability of several freely available force fields to simulate PC lipids. Where possible we have compared the simulated properties with those determined experimentally. Our results show that some of the physical properties of the lipid bilayers can depend substantially upon the simulation force field. Without additional experimental data that are in close agreement with one another, it remains almost impossible to define one force field as the 'best'. Indeed, all of the force fields considered in this study have pros and cons with respect to their ability to reproduce experimental observables. Despite this difficulty in determining one 'best' PC lipid force field, we have identified parameters that should either be avoided or used with caution. In particular, this applies to the GROMOS 53A6 POPC parameters of Kukol, 1.0 nm cut-offs (without dispersion correction) for DPPC with the Berger force field, the GROMOS43A1-S3 POPC parameters, and the use of the standard TIP3P water model with the CHARMM36 force field in GROMACS. We have also identified key areas of difference between force fields, in particular the deuterium order parameters and lipid diffusion, and it is in these properties that we suggest future improvements in some of the lipid force fields should focus upon. It should be noted that the membrane properties that are reproduced by the various force fields are not always consistent across lipid types; i.e., while a force field may accurately reproduce the behavior of one class of phospholipid, it may not do so well for other lipids. The Berger force field is a good example of this; simulations of phosphatidylethanolamine[101] and phosphatidylglycerol[102] do not compare well with experimental data. This is an important consideration when simulating bilayers containing more than one lipid species. In addition to the potential complexities of simulating non-PC lipids, the combination of appropriate membrane and protein force fields has only been studied in limited detail so far (e.g., refs 67 and 103). Future work to investigate the combinations of the lipid force fields with

dx.doi.org/10.1021/ct3003157 | J. Chem. Theory Comput. XXXX, XXX, XXX−XXX

appropriate protein force fields will be of interest to explore the successes and limitations of the various combinations that are possible, and in particular those that are widely used by the simulation community.

■ ASSOCIATED CONTENT

Supporting Information

Ten tables and seven figures containing a list of simulations, validation of the CHARMM36 force field implementation, experimental DPPC deuterium order parameters, and all results from the simulations. This information is available free of charge via the Internet at http://pubs.acs.org.

■ AUTHOR INFORMATION

Corresponding Author

*E-mail: Angel.Pineiro@usc.es, S.Khalid@soton.ac.uk. Telephone: +34-981-563-100 ext. 14042 (Á.P.), +44-2380-594176 (S.K.). Fax: +44-2380-593781 (S.K.).

Notes

The authors declare no competing financial interest.

■ ACKNOWLEDGMENTS

This work was supported by grants from the BBSRC (BB/H000658/1) and from the MICINN-Spain (MAT2011-25501). Á.P. is an Isidro Parga Pondal fellow (Xunta de Galicia). T.J.P. is funded by BBSRC grant number BB/H000658/1. We thank Hugh Larry Scott and David Poger for clarifications regarding simulation and force field parameters. We also thank Daniel Holdbrook and Jonathan Essex for valuable discussions. We wish to acknowledge use of the IRIDIS High Performance Computing Facility at the University of Southampton and the Centro de Supercomputación de Galicia (CESGA). We thank the two anonymous referees for their detailed reviews which helped to improve our study.

■ ABBREVIATIONS:

MD, molecular dynamics; DPPC, 1,2-dipalmitoyl-*sn*-glycero-3-phosphocholine; POPC, 1-palmitoyl-2-oleoyl-*sn*-glycero-3-phosphocholine; PC, phosphatidylcholine; PME, particle mesh Ewald; RF, reaction field; A_L, area per lipid; V_L, volume per lipid; K_A, isothermal area compressibility modulus; D_{HH}, bilayer thickness; DOPC, 1,2-dioleoyl-*sn*-glycero-3-phosphocholine

■ REFERENCES

(1) Straatsma, T. P.; Soares, T. A. *Proteins* **2009**, *74*, 475−488.
(2) Bond, P. J.; Faraldo-Gómez, J. D.; Sansom, M. S. P. *Biophys. J.* **2002**, *83*, 763−775.
(3) Khalid, S.; Bond, P. J.; Carpenter, T.; Sansom, M. S. P. *Biochim. Biophys. Acta, Biomembr.* **2008**, *1778*, 1871−1880.
(4) Khalid, S.; Bond, P. J.; Deol, S. S.; Sansom, M. S. P. *Proteins* **2006**, *63*, 6−15.
(5) Psachoulia, E.; Fowler, P. W.; Bond, P. J.; Sansom, M. S. P. *Biochemistry* **2008**, *47*, 10503−10512.
(6) Psachoulia, E.; Marshall, D. P.; Sansom, M. S. P. *Acc. Chem. Res.* **2009**, *43*, 388−396.
(7) Marius, P.; Leung, Y.; Piggot, T.; Khalid, S.; Williamson, P. *Eur. Biophys. J.* **2012**, *41*, 199−207.
(8) Dror, R. O.; Pan, A. C.; Arlow, D. H.; Borhani, D. W.; Maragakis, P.; Shan, Y.; Xu, H.; Shaw, D. E. *Proc. Natl. Acad. Sci. U. S. A.* **2011**, *108*, 13118−13123.
(9) Bond, P. J.; Parton, D. L.; Clark, J. F.; Sansom, M. S. P. *Biophys. J.* **2008**, *95*, 3802−3815.
(10) Sengupta, D.; Leontiadou, H.; Mark, A. E.; Marrink, S.-J. *Biochim. Biophys. Acta, Biomembr.* **2008**, *1778*, 2308−2317.
(11) Laio, A.; Parrinello, M. *Proc. Natl. Acad. Sci. U. S. A.* **2002**, *99*, 12562−12566.
(12) Hamelberg, D.; Mongan, J.; McCammon, J. A. *J. Chem. Phys.* **2004**, *120*, 11919−11929.
(13) Wang, Y.; Markwick, P. R. L.; de Oliveira, C. A. F.; McCammon, J. A. *J. Chem. Theory Comput.* **2011**, *7*, 3199−3207.
(14) Beckstein, O.; Denning, E. J.; Perilla, J. R.; Woolf, T. B. *J. Mol. Biol.* **2009**, *394*, 160−176.
(15) Perilla, J. R.; Beckstein, O.; Denning, E. J.; Woolf, T. B. *J. Comput. Chem.* **2011**, *32*, 196−209.
(16) Shimamura, T.; Weyand, S.; Beckstein, O.; Rutherford, N. G.; Hadden, J. M.; Sharples, D.; Sansom, M. S. P.; Iwata, S.; Henderson, P. J. F.; Cameron, A. D. *Science* **2010**, *328*, 470−473.
(17) Bjelkmar, P.; Niemelä, P. S.; Vattulainen, I.; Lindahl, E. *PLoS Comput. Biol.* **2009**, *5*, e1000289.
(18) Nury, H.; Poitevin, F.; Van Renterghem, C.; Changeux, J.-P.; Corringer, P.-J.; Delarue, M.; Baaden, M. *Proc. Natl. Acad. Sci. U. S. A.* **2010**, *107*, 6275−6280.
(19) Dror, R. O.; Arlow, D. H.; Maragakis, P.; Mildorf, T. J.; Pan, A. C.; Xu, H.; Borhani, D. W.; Shaw, D. E. *Proc. Natl. Acad. Sci. U. S. A.* **2011**, *108*, 18684−18689.
(20) Hess, B.; Kutzner, C.; van der Spoel, D.; Lindahl, E. *J. Chem. Theory Comput.* **2008**, *4*, 435−447.
(21) Domański, J.; Stansfeld, P.; Sansom, M.; Beckstein, O. *J. Membr. Biol.* **2010**, *236*, 255−258.
(22) Tieleman, D. P.; Berendsen, H. J. C. *J. Chem. Phys.* **1996**, *105*, 4871−4880.
(23) Anézo, C.; de Vries, A. H.; Höltje, H.-D.; Tieleman, D. P.; Marrink, S.-J. *J. Phys. Chem. B* **2003**, *107*, 9424−9433.
(24) Patra, M.; Karttunen, M.; Hyvönen, M. T.; Falck, E.; Lindqvist, P.; Vattulainen, I. *Biophys. J.* **2003**, *84*, 3636−3645.
(25) Patra, M.; Karttunen, M.; Hyvönen, M. T.; Falck, E.; Vattulainen, I. *J. Phys. Chem. B* **2004**, *108*, 4485−4494.
(26) Siu, S. W. I.; Vacha, R.; Jungwirth, P.; Böckmann, R. A. *J. Chem. Phys.* **2008**, *128*, 125103.
(27) Patra, M.; Hyvönen, M. T.; Falck, E.; Sabouri-Ghomi, M.; Vattulainen, I.; Karttunen, M. *Comput. Phys. Commun.* **2007**, *176*, 14−22.
(28) Chiu, S.-W.; Pandit, S. A.; Scott, H. L.; Jakobsson, E. *J. Phys. Chem. B* **2009**, *113*, 2748−2763.
(29) Poger, D.; van Gunsteren, W. F.; Mark, A. E. *J. Comput. Chem.* **2010**, *31*, 1117−1125.
(30) Berger, O.; Edholm, O.; Jähnig, F. *Biophys. J.* **1997**, *72*, 2002−2013.
(31) Kukol, A. *J. Chem. Theory Comput.* **2009**, *5*, 615−626.
(32) Klauda, J. B.; Venable, R. M.; Freites, J. A.; O'Connor, J. W.; Tobias, D. J.; Mondragon-Ramirez, C.; Vorobyov, I.; MacKerell, A. D.; Pastor, R. W. *J. Phys. Chem. B* **2010**, *114*, 7830−7843.
(33) Berendsen, H. J. C.; van der Spoel, D.; van Drunen, R. *Comput. Phys. Commun.* **1995**, *91*, 43−56.
(34) van der Spoel, D.; Lindahl, E.; Hess, B.; Groenhof, G.; Mark, A. E.; Berendsen, H. J. C. *J. Comput. Chem.* **2005**, *26*, 1701−1718.
(35) Parrinello, M.; Rahman, A. *J. Appl. Phys.* **1981**, *52*, 7182−7190.
(36) Nosé, S.; Klein, M. L. *Mol. Phys.* **1983**, *50*, 1055−1076.
(37) Nosé, S. *Mol. Phys.* **1984**, *52*, 255−268.
(38) Hoover, W. G. *Phys. Rev. A* **1985**, *31*, 1695−1697.
(39) Essmann, U.; Perera, L.; Berkowitz, M.; Darden, T.; Lee, H.; Pedersen, L. *J. Chem. Phys.* **1995**, *103*, 8577−8593.
(40) Pandit, S. A.; Chiu, S.-W.; Jakobsson, E.; Grama, A.; Scott, H. L. *Langmuir* **2008**, *24*, 6858−6865.
(41) Smith, L. J.; Mark, A. E.; Dobson, C. M.; van Gunsteren, W. F. *Biochemistry* **1995**, *34*, 10918−10931.
(42) van Gunsteren, W. F.; Billeter, S. R.; Eising, A. A.; Hünenberger, P. H.; Krüger, P.; Scott, W. R. P.; Tironi, I. G. *Biomolecular Simulation: The GROMOS96 Manual and User Guide*; Hochschuleverlag AG an der ETH Zürich: Zürich, 1996.

(43) Daura, X.; Mark, A. E.; van Gunsteren, W. F. *J. Comput. Chem.* **1998**, *19*, 535−547.
(44) Chiu, S. W.; Clark, M.; Balaji, V.; Subramaniam, S.; Scott, H. L.; Jakobsson, E. *Biophys. J.* **1995**, *69*, 1230−1245.
(45) National Center for Design of Biomimetic Nanoconductors. http://www.nanoconductor.org/ (accessed December 2010).
(46) Berendsen, H.; Postma, J.; van Gunsteren, W.; Hermans, J. Interaction Models for Water in Relation to Protein Hydration. In *Intermolecular Forces*; Pullman, B., Ed.; D. Reidel Publishing Company: Dordrecht, The Netherlands, 1981; pp 331−342.
(47) Poger, D.; Mark, A. E. *J. Chem. Theory Comput.* **2009**, *6*, 325−336.
(48) Schmid, N.; Eichenberger, A.; Choutko, A.; Riniker, S.; Winger, M.; Mark, A.; van Gunsteren, W. *Eur. Biophys. J.* **2011**, *40*, 843−856.
(49) Oostenbrink, C.; Villa, A.; Mark, A. E.; van Gunsteren, W. F. *J. Comput. Chem.* **2004**, *25*, 1656−1676.
(50) Lins, R. D.; Hünenberger, P. H. *J. Comput. Chem.* **2005**, *26*, 1400−1412.
(51) Soares, T. A.; Hünenberger, P. H.; Kastenholz, M. A.; Kräutler, V.; Lenz, T.; Lins, R. D.; Oostenbrink, C.; van Gunsteren, W. F. *J. Comput. Chem.* **2005**, *26*, 725−737.
(52) Tironi, I. G.; Sperb, R.; Smith, P. E.; van Gunsteren, W. F. *J. Chem. Phys.* **1995**, *102*, 5451−5459.
(53) Egberts, E.; Marrink, S.-J.; Berendsen, H. J. C. *Eur. Biophys. J.* **1994**, *22*, 423−436.
(54) Ryckaert, J.-P.; Bellemans, A. *Faraday Discuss., Chem. Soc.* **1978**, *66*, 95−106.
(55) Jorgensen, W. L.; Tirado-Rives, J. *J. Am. Chem. Soc.* **1988**, *110*, 1657−1666.
(56) Essex, J. W.; Hann, M. M.; Richards, W. G. *Philos. Trans. R. Soc. London, Ser. B* **1994**, *344*, 239−260.
(57) Tieleman, D. P.; Forrest, L. R.; Sansom, M. S. P.; Berendsen, H. J. C. *Biochemistry* **1998**, *37*, 17554−17561.
(58) Tieleman, D. P.; Sansom, M. S. P.; Berendsen, H. J. C. *Biophys. J.* **1999**, *76*, 40−49.
(59) Tieleman, D. P.; Berendsen, H. J. C.; Sansom, M. S. P. *Biophys. J.* **1999**, *76*, 1757−1769.
(60) Biocomputing at the University Of Calgary. http://moose.bio.ucalgary.ca/index.php?page=Structures_and_Topologies (accessed December 2010).
(61) Neale, C.; Bennett, W. F. D.; Tieleman, D. P.; Pomès, R. *J. Chem. Theory Comput.* **2011**, *7*, 4175−4188.
(62) Piñeiro, Á.; Bond, P. J.; Khalid, S. *Biochim. Biophys. Acta, Biomembr.* **2011**, *1808*, 1746−1752.
(63) Shirts, M. R.; Mobley, D. L.; Chodera, J. D.; Pande, V. S. *J. Phys. Chem. B* **2007**, *111*, 13052−13063.
(64) Lemkul, J. A.; Bevan, D. R. *Protein Sci.* **2011**, *20*, 1530−1545.
(65) Holdbrook, D. A.; Leung, Y. M.; Piggot, T. J.; Marius, P.; Williamson, P. T. F.; Khalid, S. *Biochemistry* **2010**, *49*, 10796−10802.
(66) Lu, R.; Niesen, M. J. M.; Hu, W.; Vaidehi, N.; Shively, J. E. *J. Biol. Chem.* **2011**, *286*, 27528−27536.
(67) Tieleman, D. P.; MacCallum, J. L.; Ash, W. L.; Kandt, C.; Xu, Z.; Monticelli, L. *J. Phys.: Condens. Matter* **2006**, *18*, S1221−S1234.
(68) Lemkul, J. A.; Bevan, D. R. *FEBS J.* **2009**, *276*, 3060−3075.
(69) Chakrabarti, N.; Neale, C.; Payandeh, J.; Pai, E. F.; Pomès, R. *Biophys. J.* **2010**, *98*, 784−792.
(70) Chandrasekhar, I.; Bakowies, D.; Glättli, A.; Hünenberger, P.; Pereira, C.; van Gunsteren, W. F. *Mol. Simul.* **2005**, *31*, 543−548.
(71) Chandrasekhar, I.; Kastenholz, M.; Lins, R. D.; Oostenbrink, C.; Schuler, L. D.; Tieleman, D. P.; van Gunsteren, W. F. *Eur. Biophys. J.* **2003**, *32*, 67−77.
(72) Bachar, M.; Brunelle, P.; Tieleman, D. P.; Rauk, A. *J. Phys. Chem. B* **2004**, *108*, 7170−7179.
(73) GROMACS Users Forum - POPC 53a6 topology (dihedral multiplicity). http://gromacs.5086.n6.nabble.com/POPC-53a6-topology-dihedral-multiplicity-tp4441475p4441482.html (accessed June 2012).
(74) Piggot, T. J.; Holdbrook, D. A.; Khalid, S. *J. Phys. Chem. B* **2011**, *115*, 13381−13388.
(75) Klauda, J. B.; Brooks, B. R.; MacKerell, A. D.; Venable, R. M.; Pastor, R. W. *J. Phys. Chem. B* **2005**, *109*, 5300−5311.
(76) Pastor, R. W.; MacKerell, A. D. *J. Phys. Chem. Lett.* **2011**, *2*, 1526−1532.
(77) Bjelkmar, P.; Larsson, P.; Cuendet, M. A.; Hess, B.; Lindahl, E. *J. Chem. Theory Comput.* **2010**, *6*, 459−466.
(78) Phillips, J. C.; Braun, R.; Wang, W.; Gumbart, J.; Tajkhorshid, E.; Villa, E.; Chipot, C.; Skeel, R. D.; Kalé, L.; Schulten, K. *J. Comput. Chem.* **2005**, *26*, 1781−1802.
(79) Laboratory of Molecular & Thermodynamic Modeling. http://terpconnect.umd.edu/~jbklauda/index.html (accessed December 2010).
(80) Brooks, B. R.; Brooks, C. L.; Mackerell, A. D.; Nilsson, L.; Petrella, R. J.; Roux, B.; Won, Y.; Archontis, G.; Bartels, C.; Boresch, S.; et al. *J. Comput. Chem.* **2009**, *30*, 1545−1614.
(81) Jorgensen, W. L.; Chandrasekhar, J.; Madura, J. D.; Impey, R. W.; Klein, M. L. *J. Chem. Phys.* **1983**, *79*, 926−935.
(82) Durell, S. R.; Brooks, B. R.; Ben-Naim, A. *J. Phys. Chem.* **1994**, *98*, 2198−2202.
(83) Neria, E.; Fischer, S.; Karplus, M. *J. Chem. Phys.* **1996**, *105*, 1902−1921.
(84) Steinbach, P. J.; Brooks, B. R. *J. Comput. Chem.* **1994**, *15*, 667−683.
(85) Jo, S.; Kim, T.; Im, W. *PLoS ONE* **2007**, *2*, e880.
(86) CHARMM-GUI. http://www.charmm-gui.org/?doc=archive&lib=lipid_pure (accessed June 2012).
(87) Flyvbjerg, H.; Petersen, H. G. *J. Chem. Phys.* **1989**, *91*, 461−466.
(88) Niemelä, P. S.; Miettinen, M. S.; Monticelli, L.; Hammaren, H.; Bjelkmar, P.; Murtola, T.; Lindahl, E.; Vattulainen, I. *J. Am. Chem. Soc.* **2010**, *132*, 7574−7575.
(89) Nagle, J. F.; Tristram-Nagle, S. *Biochim. Biophys. Acta, Rev. Biomembr.* **2000**, *1469*, 159−195.
(90) Petrache, H. I.; Dodd, S. W.; Brown, M. F. *Biophys. J.* **2000**, *79*, 3172−3192.
(91) Seelig, J.; Waespe-Šarčević, N. *Biochemistry* **1978**, *17*, 3310−3315.
(92) Warschawski, D.; Devaux, P. *Eur. Biophys. J.* **2005**, *34*, 987−996.
(93) Büldt, G.; Gally, H. U.; Seelig, J.; Zaccai, G. *J. Mol. Biol.* **1979**, *134*, 673−691.
(94) Ulmschneider, J. P.; Ulmschneider, M. B. *J. Chem. Theory Comput.* **2009**, *5*, 1803−1813.
(95) Sapay, N.; Tieleman, D. P. *J. Comput. Chem.* **2011**, *32*, 1400−1410.
(96) de Vries, A. H.; Chandrasekhar, I.; van Gunsteren, W. F.; Hünenberger, P. H. *J. Phys. Chem. B* **2005**, *109*, 11643−11652.
(97) Castro-Román, F.; Benz, R. W.; White, S. H.; Tobias, D. J. *J. Phys. Chem. B* **2006**, *110*, 24157−24164.
(98) Klauda, J. B.; Brooks, B. R.; Pastor, R. W. *J. Chem. Phys.* **2006**, *125*, 144710.
(99) Lange, O. F.; van der Spoel, D.; de Groot, B. L. *Biophys. J.* **2010**, *99*, 647−655.
(100) Marrink, S.; Lindahl, E.; Edholm, O.; Mark, A. *J. Am. Chem. Soc.* **2001**, *123*, 8638−8639.
(101) de Vries, A. H.; Mark, A. E.; Marrink, S. J. *J. Phys. Chem. B* **2004**, *108*, 2454−2463.
(102) Hénin, J.; Shinoda, W.; Klein, M. L. *J. Phys. Chem. B* **2009**, *113*, 6958−6963.
(103) Cordomí, A.; Caltabiano, G.; Pardo, L. *J. Chem. Theory Comput.* **2012**, *8*, 948−958.
(104) Nagle, J. F.; Zhang, R.; Tristram-Nagle, S.; Sun, W.; Petrache, H. I.; Suter, R. M. *Biophys. J.* **1996**, *70*, 1419−1431.
(105) Kučerka, N.; Nagle, J. F.; Sachs, J. N.; Feller, S. E.; Pencer, J.; Jackson, A.; Katsaras, J. *Biophys. J.* **2008**, *95*, 2356−2367.
(106) Kučerka, N.; Nieh, M.-P.; Katsaras, J. *Biochim. Biophys. Acta, Biomembr.* **2011**, *1808*, 2761−2771.
(107) Kučerka, N.; Tristram-Nagle, S.; Nagle, J. F. *Biophys. J.* **2006**, *90*, L83−L85.
(108) Smaby, J. M.; Momsen, M. M.; Brockman, H. L.; Brown, R. E. *Biophys. J.* **1997**, *73*, 1492−1505.

(109) Hyslop, P. A.; Morel, B.; Sauerheber, R. D. *Biochemistry* **1990**, *29*, 1025−1038.
(110) Kučerka, N.; Tristram-Nagle, S.; Nagle, J. *J. Membr. Biol.* **2005**, *208*, 193−202.
(111) Binder, H.; Gawrisch, K. *J. Phys. Chem. B* **2001**, *105*, 12378−12390.
(112) Kuo, A.-L.; Wade, C. G. *Biochemistry* **1979**, *18*, 2300−2308.
(113) Wu, E.; Jacobson, K.; Papahadjopoulos, D. *Biochemistry* **1977**, *16*, 3936−3941.
(114) Sheats, J. R.; McConnell, H. M. *Proc. Natl. Acad. Sci. U. S. A.* **1978**, *75*, 4661−4663.
(115) Köchy, T.; Bayerl, T. M. *Phys. Rev. E* **1993**, *47*, 2109−2116.
(116) Filippov, A.; Orädd, G.; Lindblom, G. *Langmuir* **2003**, *19*, 6397−6400.
(117) Ladha, S.; Mackie, A. R.; Harvey, L. J.; Clark, D. C.; Lea, E. J.; Brullemans, M.; Duclohier, H. *Biophys. J.* **1996**, *71*, 1364−1373.